UNIVERSITY OF TURKU

Enhancing Supercapacitor Performance with Chemically Synthesised RGO/CeO_2/PEDOT Nanocomposite.

Jayanthi Lakshmipathy

Master's Thesis

Materials Chemistry

Department of Chemistry

Supervisors:

Dr. Mikko Salomäki

Prof. Carita Kvarnström

13.06.2025

Turku

Using the Turnitin Originality Check service, the originality of this thesis has been verified in compliance with the University of Turku's quality assurance system.

Master's Thesis

Subject: Materials Chemistry
Programme: Master's Degree Programme in Materials Chemistry
Author: Jayanthi Lakshmipathy
Title: Enhancing Supercapacitor Performance with Chemically synthesised RGO/CeO_2/PEDOT Nanocomposite.
Supervisor: Dr. Mikko Salomäki, Prof. Carita Kvarnström
Number of pages: 54 pages
Date: June 2025

Abstract

Supercapacitors exhibit exceptional power density, rapid charging and discharging capabilities, and long-term cycling stability, making them promising candidates for energy storage solutions; nonetheless, their electrochemical efficiency is profoundly influenced by the choice and design of electrode materials.[1] The creation and characterization of high-performance nanocomposite electrode material for supercapacitor applications are examined in this thesis, focusing on the combination of reduced graphene oxide (RGO) which offers high conductivity and huge surface area, cerium oxide (CeO_2) provides redox-active sites, and poly(3,4-ethylenedioxythiophene) (PEDOT) enhances conductivity and pseudocapacitance. RGO/CeO_2 and RGO/CeO_2/PEDOT nanocomposites were synthesised using in-situ oxidation-reduction technique and chemical polymerization method. The prepared RGO, RGO/CeO_2 and RGO/CeO_2/PEDOT nanocomposites were thoroughly characterised by using UV-visible spectroscopy, Raman spectroscopy, and XPS. The electrochemical behaviour of fabricated supercapacitors was examined through cyclic voltammetry (CV) and galvanostatic charge-discharge (GCD) techniques using a three-electrode cell setup under 0.5 M H_2SO_4 electrolyte. The RGO/CeO_2/PEDOT supercapacitor demonstrated greater energy and power densities, as well as a much higher specific capacitance of 150 F/g at a current density of 0.4 A/g as compared to individual RGO and RGO/CeO_2 composite. These findings highlight the synergistic effect of combining conducting polymers, metal oxides, and carbon materials, and they show the potential of the RGO/CeO_2/PEDOT nanocomposite as an efficient electrode material for next generation supercapacitors.

Keywords: Reduced graphene oxide, cerium oxide, PEDOT, supercapacitor.

Acknowledgement

Here, I want to sincerely thank my supervisors, Prof. Carita Kvarnström and Dr. Mikko Salomäki, for their important help over the entire experimental research. This experimental work proceeded smoothly thanks to the guidance, vast operating experience, and professional understanding of Dr. Mikko Salomäki. Insightful advice and support from Prof. Carita Kvarnström were also very beneficial to my thesis work. I am incredibly appreciative of their dedication, tolerance, and guidance, all of which were crucial in helping me get beyond several challenges throughout the project.

Abbreviations and Terms

RT	Room Temperature
RGO	Reduced graphene oxide
GO	Graphene oxide
PEDOT	poly (3,4-ethylenedioxythiophene)
EDOT	3,4-ethylenedioxythiophene
CeO_2	Cerium Oxide
EDLC	Electric double layer capacitor
CPs	Conducting Polymers
CV	Cyclic Voltammetry
GCD	Galvanostatic charge-discharge
NMP	N-methyl-2-pyrrolidone
CVD	Chemical Vapor deposition
MOF	Metal Organic Framework

Table of Contents

1. Introduction

Because of its vital significance in both the industrial and home sectors, energy is still a crucial concern. The world economy's explosive expansion has sped up the depletion of fossil fuel supplies, creating two main problems; the imminence of these limited energy sources' scarcity and the worsening of environmental pollution brought on by rising greenhouse gas emissions. These changes highlight how important it is to reduce the use of fossil fuels and switch to greener energy sources in order to lessen the long-term effects on the ecosystem. As a result, the growth and trading of environmentally benign renewable energy sources, together with the related technologies, are of the greatest significance.[1,2] It is necessary to develop technologies that can efficiently store energy and provide it when needed. In this regard, energy storage devices can be used to mitigate the growing global demand for electricity. In addition to meeting the needs for energy use across a range of industries, these gadgets offer a sustainable and environmentally responsible substitute for conventional energy sources.[3]

Among the most crucial types of energy storage systems are batteries, fuel cells, and supercapacitors. Fuel cells, and batteries utilize redox processes at the electrodes to convert chemical power into electrical power, but they contrast in that fuel cell devices demand an uninterrupted supply of fuel in order to work properly. Fuel cells are open networks having physically segregated energy storage and conversion of energy compartments, whereas batteries are closed systems since energy conversion and storage take place in a single compartment.[4] An electric double layer (EDL) at the electrode and electrolyte interface is the main mechanism by which supercapacitors receive and remove ions to preserve and distribute energy. They are more efficient, have longer lifespan, a larger specific capacitance, and a higher power density. With negligible degradation, they can withstand thousands of charge/discharge cycle segments. They are also skilled at combining the energy density features of batteries with the power

release capabilities of capacitors. These features make supercapacitors an outstanding piece of solution that overcomes the separation between batteries and capacitors to produce a system that is remarkably efficient and compact.[5,6]

Table 1 discusses the electrical properties of capacitors, batteries, and supercapacitors, and Figure 1 displays a Ragone plot analysing the features of fuel cells, batteries, and supercapacitors.[7]

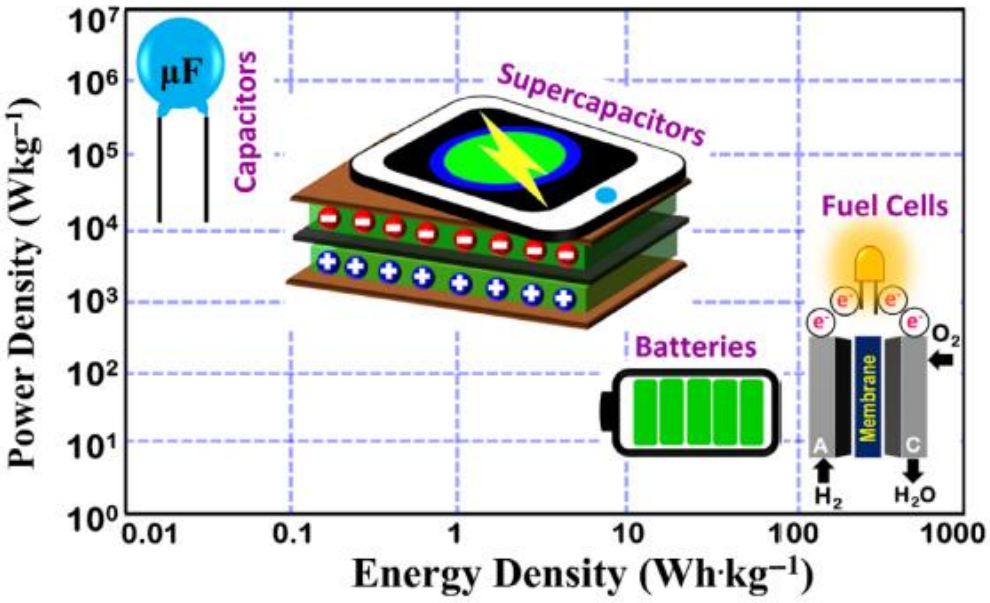

Figure 1 Ragone plot comparing power density against energy density.[7]

As seen in Figure 1, a battery may produce as much as 150 Wh/Kg of energy, which is roughly 10 times the capacity of supercapacitors. Supercapacitor power density demands are not fulfilled by the batteries. Batteries only just manage to reach 200 W/Kg, almost 20 times less than the expected electrochemical capacitor's output.[8] Furthermore, the batteries have drawbacks such short charge-discharge cycles or sharp output drops brought on by cold ambient temperatures. It has a short lifespan and is expensive to manage. Today, these supercapacitors cannot be utilized for replacing the technology of batteries, however, they might serve as substitutes by providing the immediate voltage required to lower battery current in the event of a brief and transient power outage. Aside from this, bulk

battery systems can use parallel-mounted electrochemical supercapacitors to compensate for brief and transient interruptions.[9,10]

Table.1 Capacitors, supercapacitors, and batteries' electrochemical properties.[7]

Electrochemical Properties	Supercapacitors	Capacitors	Batteries
Power density (Wh/Kg)	1000-2000	>10000	<1000
Energy density (W/Kg)	1-10	<0.1	10-100
Charge time (s)	1-30	10^{-6}–10^{-3}	1080-10800
Discharge time (s)	1-30	10^{-6}–10^{-3}	3600-18000
Charge/Discharge efficiency	0%-95%	100%	-
Cycle life	>100,000	>500,000	<1000

1.1 Supercapacitors

A class of energy storage devices known as supercapacitors holds great promise for combining increased energy density with the high energy production found in traditional dielectric capacitors and batteries.[11]A permeable insulator separates the two identical electrodes, which are submerged in a solution of electrolytes. Supercapacitors are referred to as symmetric when both of the electrodes are of the same kind, and asymmetric when the electrode patterns are different. Supercapacitors can be categorized into two primary types; electrical double layer capacitors (EDLCs) and pseudocapacitors depending on how they store energy.[12]

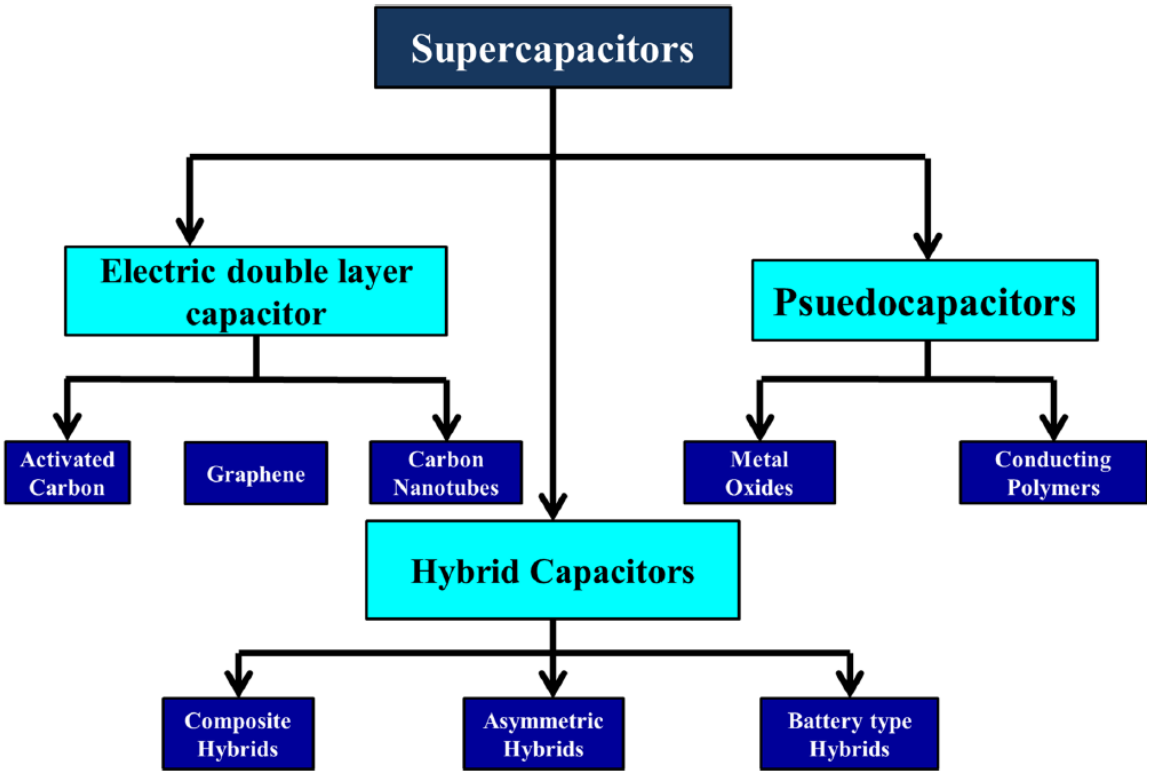

Figure 2 Classification of Supercapacitors.[7]

1.1.1 Electric double layer capacitors (EDLCs)

An electrolyte, two carbon-based electrode materials, and a separator comprise EDLCs. There is no need for charge transfers between the electrolyte and electrode because EDLC may store charges either electrostatically or non-Faradic. The electric double layer is the kind of energy storage methodology used by EDLCs.[13] Since electrolyte ions travel across the separator and on the oppositely charged electrode pores as a result of oppositional charge repulsion brought on by the potential variation, there was actually no build-up of charges on the outer layer of the electrode when current was utilized (Figure 3). In order to prevent ion collision in electrodes, e double layer of charges was created. Along with improving a particular surface area while minimizing the space between the electrodes, the double layer enables EDLCs to attain high densities of energy.[14,15] Additionally, the stotage mechanism of EDLCs makes it possible for superior power output, quick energy intake, and distribution. Given that EDLCs can

sustain millions of cycles while batteries may only withstand a few thousand, since the no-faradic phase isn't a chemical process, there may be some apparent distinctions between the two kinds of batteries. Additionally, the method of charging does not require an electrolyte solvent; with batteries made with Li-ion cells, the solidified electrolyte inter-phase happens when graphite cathods are utilized. Graphene, activated carbon, and carbon nanotubes are examples of highly porous carbon materials that are frequently used to make EDLCs.[16,9]

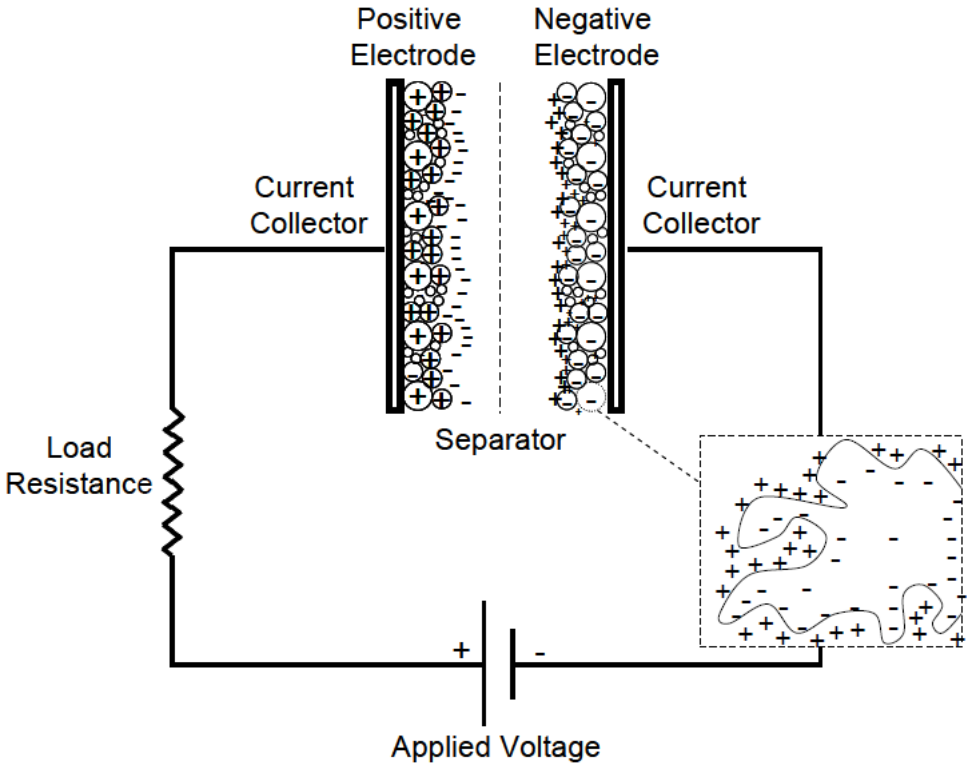

Figure 3 Schematic illustration of EDLC.[15]

1.1.2 Pseudocapacitors

Pseudocapacitors store energy by use of quick and reversible (faradaic) reactions at the electrode material's surface. They are also a kind of supercapacitor and use the fast redox reactions to increase capacitance and energy density in contrast to EDLCs, which rely on electrostatic charge separation. Faradaic processes, in which electron charge transfer takes place between the electrode and electrolyte, resulting in oxidation-reduction reactions, are the basis for the workings of

pseudocapacitors. The total capacitance is influenced by the processes, which occur at or close to the electrode material's surface. The following reaction can be used to explain the energy storage method.

$$M^{n+} + e^- \leftrightarrow M^{(n-1)+}$$

Where 'M' denotes the electroactive material on the electrode surface. Compared to EDLCs, pseudocapacitors can store more energy due to the faradaic nature of these reactions. A range of materials capable of quick and reversible redox reactions are used in pseudocapacitors. Usually, these materials consist of transition metal oxides and conducting polymers.[17]

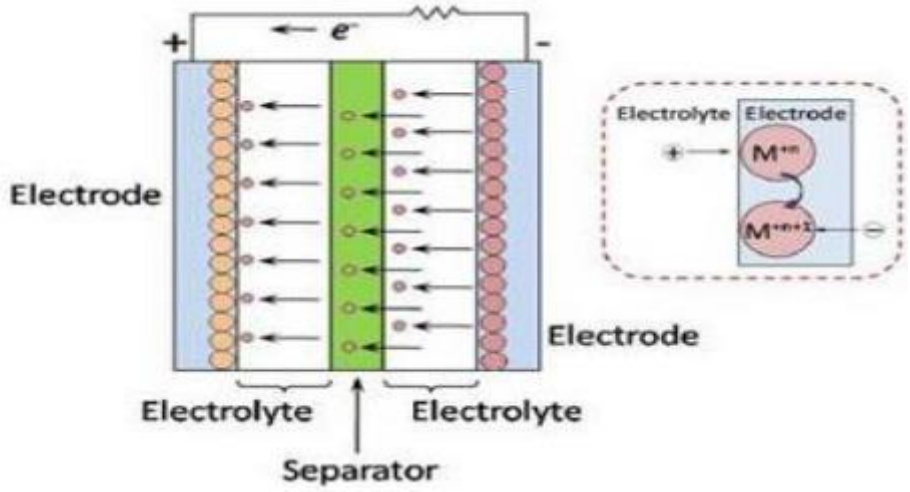

Figure 4 A schematic representation of pseudocapacitors.[17]

1.2 Graphene (Carbon Materials)

Kostantin Novoselov and Andre Geim used the mechanical exfoliation method, also referred to as the scotch tape technique, to successfully separate monolayer graphene, a carbon crystallite that is one atom thick, from bulk graphite in 2004. For a more thorough analysis, they next placed these graphene flakes on thin silicon dioxide layers on top of silicon wafers. They were awarded the 2010 Nobel prize in physics for their pioneering work that uncovered the extraordinary

physical characteristics of graphene, underscoring the revolutionary influence of their discovery on the field of nanomaterials science.[18,19]

A single layer of carbon atoms arranged in a two-dimensional honeycomb lattice makes up graphene, a nanomaterial. Each carbon atom is joined to three others by sp^2 hybridization to form a planar structure that is one atom thick. With carbon atoms taking up locations where hydrogen atoms would normally be found in benzene molecules, this lattice can be seen as a network of interconnected hexagonal rings that resemble benzene. Because graphene lacks functional groups that include oxygen, it has hydrophobic properties. Composed of atoms bound together by sp^2 hybridization, graphene is a 2D allotrope of carbon with a distinctive C-C bond length of roughly 0.142 nm. Graphite-like structures are created when individual graphene layers stack together, with an interlayer gap of roughly 0.333 nm between them.[20,21]

A weak van der walls force holds single honeycomb graphitic lattice layers together, forming 3D bulk graphite. This honeycomb lattice is the basic component of all carbon nanostructures, consisting of a single graphitic layer with covalently customized sp^2 connected carbon atoms arranged in a hexagonal pattern. When the graphite is sphere-like structure, it is known as 0-D fullerene; when it rotates along its axis, it is a 1D nanotube; and when it has a flat 2D structure between one or more assembled layers, it is called graphene. Due to its unique remarkable electrical and mechanical capabilities, both of which are a result of strong planar σ bonds.[22]

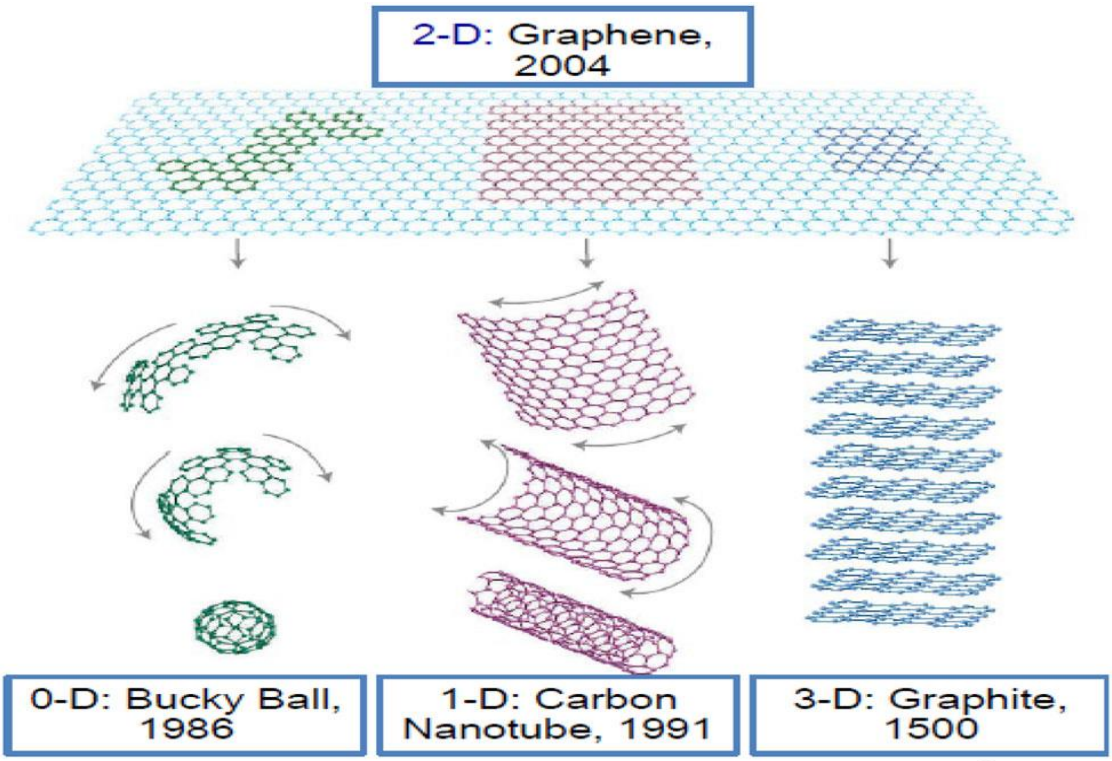

Figure 5 Different features of carbon nanomaterials which are 2-D graphene, 0-D fullerene, 1-D carbon nanotube and 3-D graphite.[22]

There are two primary methods for producing graphene; top-down and bottom-up. Graphene films are created by dissecting raw graphite using top-down techniques. These include chemical synthesis, mechanical exfoliation, and chemical exfoliation. Pyrolysis, epitaxial growth, chemical vapor deposition, and other innovative methods are instances of bottom-up strategies that create graphene from atomic or molecule precursors. Graphene has been considered the thinnest elastic crystal that possesses good thermal conductivity and high electron mobility. Graphene came into prominence quite quickly in various applications from optoelectronic devices, biomaterials and bionics, energy storage and batteries, electrochemical performance, thermal management, etc.[23]

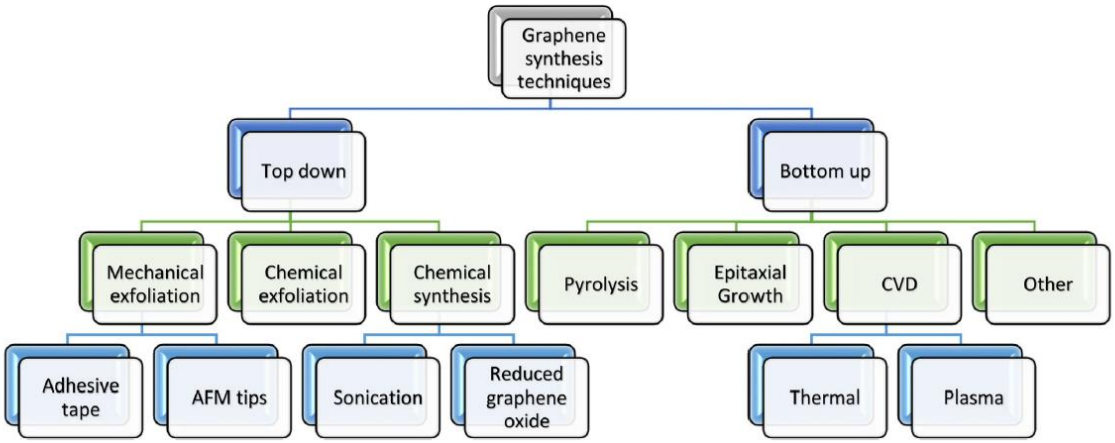

Figure 6 Graphene synthesis techniques.[23]

1.3 Metal Oxides

Another crucial class of materials that has been extensively studied for supercapacitor electrodes are metal oxides. They are appealing candidates for improving energy storage capacity and performance in supercapacitors due to their special qualities, including pseudocapacitance resulting from reversible redox processes. Cobalt oxide (Co_3O_4), Cerium oxide (CeO_2), Nickel oxide (NiO), Ruthenium oxide (RuO_2), Manganese oxide (MnO_2) and Vanadium oxide (V_2O_5) are the dominant transition metal oxides that are being investigated presently for pseudocapacitors electrodes. A rise in capacitance occurs because these metal oxides are undergoing more than one oxidation state at some potentials. Ruthenium oxide (RuO_2) in amorphous and crystalline forms, RuO_2 is highly important for theoretical and practical applications based on its varying characteristics like metallic conductivity, catalytic activities, chemical stability and heat resistance at high levels, electrochemical redox properties and field emitting characteristics.[24] RuO_2 is extensively utilized in numerous sectors such as metallic thin-film tools, electronic parts, electronic circuit production, and the fabrication of light and robust film resistance. Manganese Oxide (MnO_2) is the subject of numerous studies because of its unique chemical and physical properties, which have numerous uses in molecular adsorption storage, ion

exchange, catalysis and biosensors. Its low cost, good capacitive performance in aqueous electrolytes, and environmental friendliness made it an extremely important electrode material for supercapacitors. Since it is inexpensive, easy to synthesize, and environmentally benign, nickel oxide (NO) is regarded as a crucial electrode material for supercapacitors. In capacitor technology, metal oxides play a key role in improving energy storage capacity. The approximate consumption breakdown of various metal oxides is based on prevalent trends and applications can be determined, as shown in Figure 7. Metal oxides-based electrodes have advanced as a result of ongoing research efforts to maximize their cyclability and capacitive behaviour.[25]

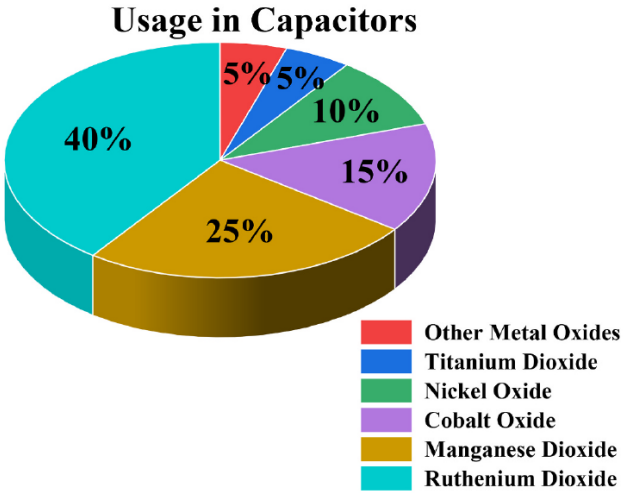

Figure 7 Percentage (%) distribution of metal oxides used in the supercapacitor.[25]

1.4 Conducting Polymers

Supercapacitors use conducting polymers (CPs) owing to their enormous capacitance, low analogous series resistance, and outstanding electrical conductivity. They are suitable for boosting capacitance through their intrinsic massive surface area and capacity to store power using redox processes. Furthermore, metallic conductivity, a widely requested property for electrode materials in supercapacitor applications, can be obtained by chemically doping

CPs. CPs are considered the most promising pseudocapacitive material because to their unique structural arrangement and properties. These polymers consistent conjugated backbones enable effective delocalization of π electrons throughout the chain. They use redox reactions, also known as doping and de-doping, to store and deliver charges, Figure 8 illustrates this mechanism. This reversible process enables CPs to change their conductivity and function as conductors, semiconductors, or insulators. Ions are moved to the polymer backbone during the oxidation or doping, whereas they are released into the solution during the reduction or de-doping process. Charging happens throughout the material, not only on the surface, resulting in higher specific capacitance compared to carbon electrodes.[26,27]

Additionally, CPs can be structurally modified to improve characteristics and manage doping levels for better conductivity. Their mechanical characteristics, biodegradability, and eco-friendliness make them suitable for wearable electronics, lightweight and flexible supercapacitors, and bio-implants. Polyaniline, polythiophene, polypyrrole, and poly (3,4- ethelenedioxythiophene) (PEDOT) are the most widely used conducting polymers. CPs are extremely adaptable and appropriate for an extensive number of applications because of their variable electrical conductivity, measurable chemical and electrostatic actions, malleability, chemical resistance, simple creation, and extreme biocompatibility. For instance, because of their flexibility, light weight, and compatibility with low-cost production processes, CPs can be utilized as crucial parts of devices like organic solar cells, light-emitting diodes (LEDs), and organic field-effect transistors (OFETs). Moreover, CPs can offer a sizable charge storage capacity, quick charging and discharging rates, and enhanced cycling stability when employed as active materials for electrodes in energy storage devices.[27,28]

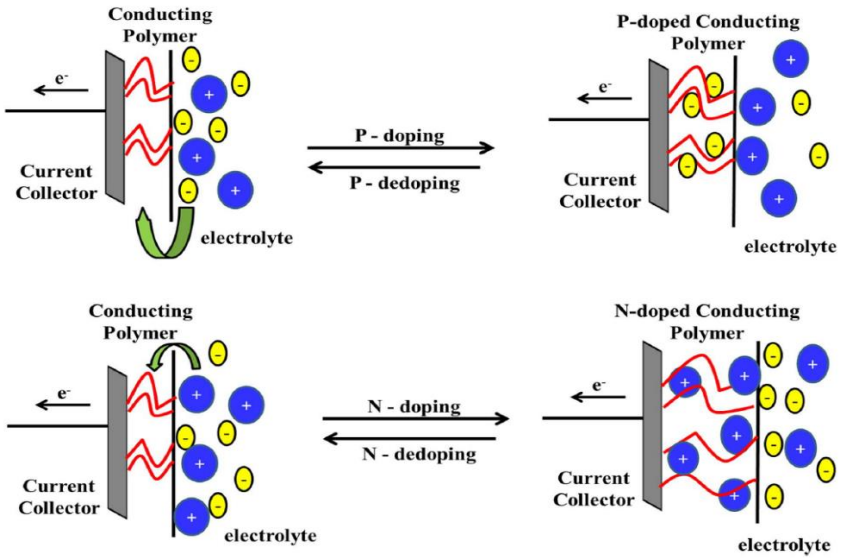

Figure 8 Process of charge-discharge in electrodes of N and P doped polymers.[28]

1.5 Application of supercapacitors.

Applications requiring significant power density, multiple charge/discharge cycles, and long running lifespans benefit greatly from supercapacitors. They are extensively utilized in many different fields, including as electronic gadgets, wind energy systems, mobile communication infrastructure, and industrial processes. Electric vehicles, uninterruptible power supply (UPS), and other power electronics systems have adopted them due to their improved performance over lead-acid batteries. Supercapacitors have also been included into hybrid and renewable energy systems in recent years to improve grid regulation and voltage stability. They are perfect for powering portable gadgets like speakers and camera flashes because of their quick charging speed. Supercapacitors can lower energy use and CO_2 emissions in the transportation sector, expecially when used in conjunction with regenerative braking systems. Consumer electronics, power tools backup power sources, microgrids, renewable energy storage, street lighting, medical equipment, military systems, and automotive technology are just a few examples of their many uses.[29] A number of real-world uses for supercapacitors in different fields are shown in Figure 9.

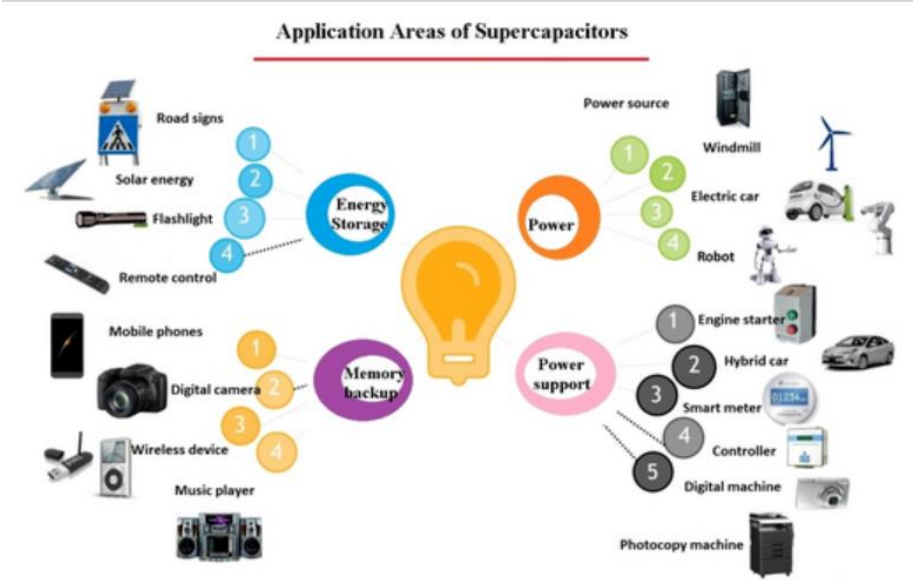

Figure 9 Some examples of supercapacitor applications.[30]

1.6 Electrode materials for Supercapacitors.

1.6.1 Reduced graphene oxide (RGO)

A flexible material with remarkable properties, reduced graphene oxide (RGO) provides a link between graphene and its predecessor, graphene oxide (GO). GO, which is created by oxidizing and exfoliating graphite, is reduced to produce it. The reduction procedure restores the sp^2 carbon network and partially restores graphene-like properties by removing oxygen-containing functional groups from the graphene oxide sheets, such as epoxides, hydroxyls, and carboxyls. In terms of mechanical, optoelectronic, and conductive properties, RGO is similar to pristine graphene because of its heterogeneous structure, which includes regions with oxygen groups and a graphene-like basal plane embellished with structural imperfections. Because of its graphene-like characteristics, RGO is highly prized and can be used in a wide range of applications, such as energy storage systems, sensors, environmental and medicinal gadgets, and catalytic processes.[31]

RGO can be synthesized using a variety of reduction techniques, including as chemical reduction, thermal reduction, hydrothermal reduction, and electrochemical reduction. By controlling the synthesized RGO's degree of reduction, structure, and properties, these methods enable tailored designs for particular uses. The removal of oxygen functional groups converts GO into RGO, as seen in Figure 10. Chemical reduction is a simple and affordable process that can be used with modest heating or at room temperature. This method usually relies on the use of chemicals such as ascorbic acid and hydrazine. Quick annealing at high temperatures is necessary for thermal reduction techniques, which expand the CO or CO_2 gases produced by the degradation of oxygen functional groups in order to extract GO.[31,32]

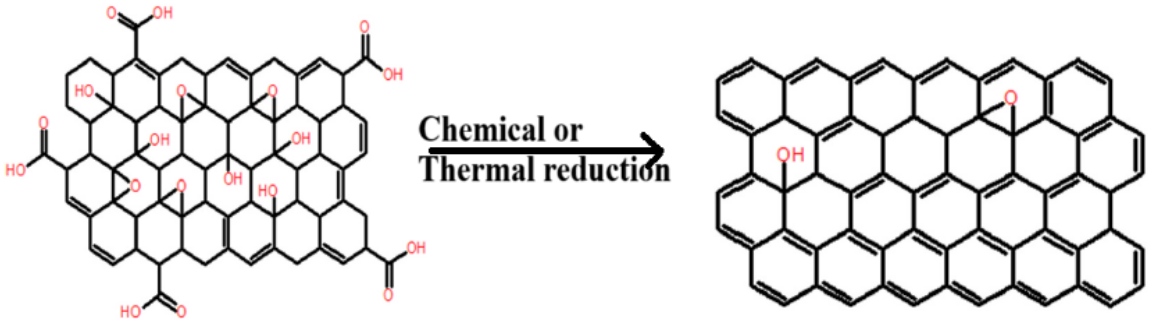

Figure 10 Structure of GO to RGO.

1.6.2 Cerium Oxide (CeO_2)

Cerium oxide (CeO_2), a rare earth metal oxide, has garnered more attention than other materials being investigated for supercapacitor electrodes because to its environmental tolerance, structural plasticity, and pseudocapacitive qualities. CeO_2 takes on a cubic crystal structure of the fluorite type, with eight O^{2-} ions around the Ce^{4+} ions. This material's capacity to transition between states is one of its distinctive states is one of its distinctive qualities. The partially filled 4f orbital gives the material this redox flexibility, which enables reversible redox

processes that are essential to pseudocapacitive behaviour. The following reaction is a simplified version of the redox process.[33]

Non-faradaic reaction

(CeO_2) surface + $M^+ + e^- \rightleftharpoons (CeO_2 \cdot M^+)$ surface

Faradaic reaction

$CeO_2 + M^+ + e^- \rightleftharpoons CeO_2M$

In the redox reactions, M^+ stands for an alkali metal ion (Na^+, K^+, etc.) that is engaged in charge balancing. Oxygen vacancies are also formed during this transition between Ce^{4+} and $Ce^{3+,}$ which improves ionic and electrical conductivity. Gap states created by these oxygen vacancies promote charge delocalization and electron mobility throughout the lattice.[33,34]

The electrochemical behaviour of CeO_2 is highly dependent on its shape, particle size, and surface area. Nanorods, nano cubes, and nanoparticles have been synthesised using the hydrothermal and solvothermal methods. Among them, nanorods tend to perform better due to greater specific surface area and exposure of more active crystal planes with higher redox activity.[35]

CeO_2 nanostructures can be synthesised using a variety of wet chemical methods such as, hydrothermal synthesis, sol-gel and co-precipitation procedures, and combustion of sacrificial metal-organic frameworks (MOFs) to generate porous CeO_2 morphology. MOF derived CeO_2 has been reported to exhibit specific capacitances of 1204 Fg^{-1} in redox-active electrolytes, demonstrating the great potential of this method. Although CeO_2 is a very promising pseudocapacitive electrode material, its application remains limited by, poor conductivity, moderate energy density compared to battery-type materials, and hybridization requirement with conductive additives. Figure 11 illustrates the crystal structure of cerium oxide.[36]

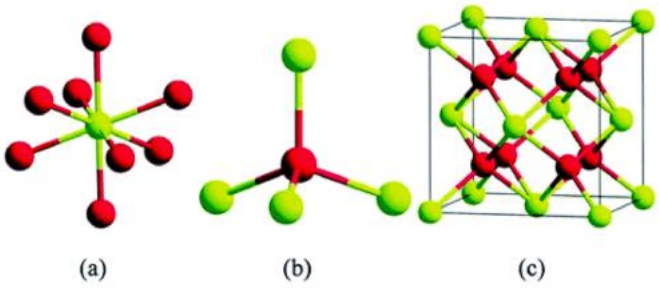

Figure 11 is depicted the Ce_4O_8 unit cell structure, (a) Eight-fold organized cerium atoms in yellow, (b) Four-fold oxygen atoms in red, (c) The basic fluorite lattice.[33]

1.6.3 PEDOT

A highly conducting and electroactive polymer, poly(3,4-ethylenedioxythiophene) (PEDOT) has solidified its position as a top candidate for supercapacitor electrode materials. PEDOT's distinctive blend of high electrical conductivity, exceptional environmental stability, mechanical flexibility, and noticeable pseudocapacitve behaviour is for its worldwide popularity. The performance of next generation supercapacitors, particularly hybrid and ternary nanocomposite-based devices like as integrating RGO and CeO_2, can be strategically improved PEDOT as an electrode material. PEDOT is an extremely versatile conducting polymer of significant interest in academic studies as well as industrial uses. PEDOT has some favourable aspects compared to other polythiophene derivatives. PEDOT is more stable in its oxidised state and has a small bandgap and low oxidative capability. It belongs to the family of conjugated polymers and has a backbone made up of two types of bonds that interchange. Due to the unique stacking of the thiophene rings connected through ethylenedioxy linkers, the distribution of the π-electrons in PEDOT is extremely efficient and results in a high electrical conductivity.[37]

PEDOT has been synthesized via a wide range of methods that endow specific morphological and electrochemical characteristics essential for supercapacitor

applications. Vapor-phase approaches, electrochemical polymerization, and chemical oxidative polymerization are notable PEDOT synthesis processes. The most common and industrially substantial method is oxidative polymerization. According to this method, the EDOT monomer is oxidatively polymerized in the presence of oxidizers such as $FeCl_3$ in present or absent conditions. One of the interesting alternatives is surfactant-free interfacial polymerization, in which PEDOT grows between two immiscible liquids, the technique produces robust, conductive films. Electrochemical polymerization involves the application of an oxidative potential to a working electrode located within an EDOT containing electrolyte. This facilitates precise control over the thickness and morphology of PEDOT films.[37]

Hydrothermal synthesis has also been employed in the specific case of PEDOT based composites. Here a precursor solution containing EDOT and other components. Vapor phase polymerization is another method applied in PEDOT synthesis, where a film containing the oxidant mixed with pyridine is exposed to EDOT vapours for initiating the polymerization process. This method is superior to chemical synthesis since it employs a bottom-up approach in which the monomers are positioned in an orderly arranged to produce a highly ordered crystalline structure.[37,38]

The most common and quickly growing use of PEDOT is in electrochemical energy storage, namely as a supercapacitor electrode material. PEDOT based electrodes have excellent pseudocapacitive behaviour because to their ability to undergo redox processes, which improves specific capacitance and rate performance. PEDOT can be used in flexible and stretchable electronics because of its mechanical strength, especially in thin film and composite forms. Under extreme bending, stretching, or twisting, PEDOT-coated films and sheets maintain their excellent conductivity. These characteristics are being used to create next generation smart clothing, conformal sensors, and textiles with

integrated energy storage. PEDOT is commonly used as a conducting binder or coating in hybrid electrodes, which significantly improves the functionality of devices based on metal oxides or carbon nanostructures. A wide range of innovative uses, including energy storage, flexible and wearable technology, optoelectronics, sensors, and bio-interfaces, make use of PEDOT's multifunctionality. PEDOT is positioned as a key component for the future generation of high performance, multipurpose electronic and energy systems due to its versatility in synthesis, which allows it to be created in a range of morphologies and composite structures while maintaining its mechanical integrity and exceptional electrical qualities.[39,40]

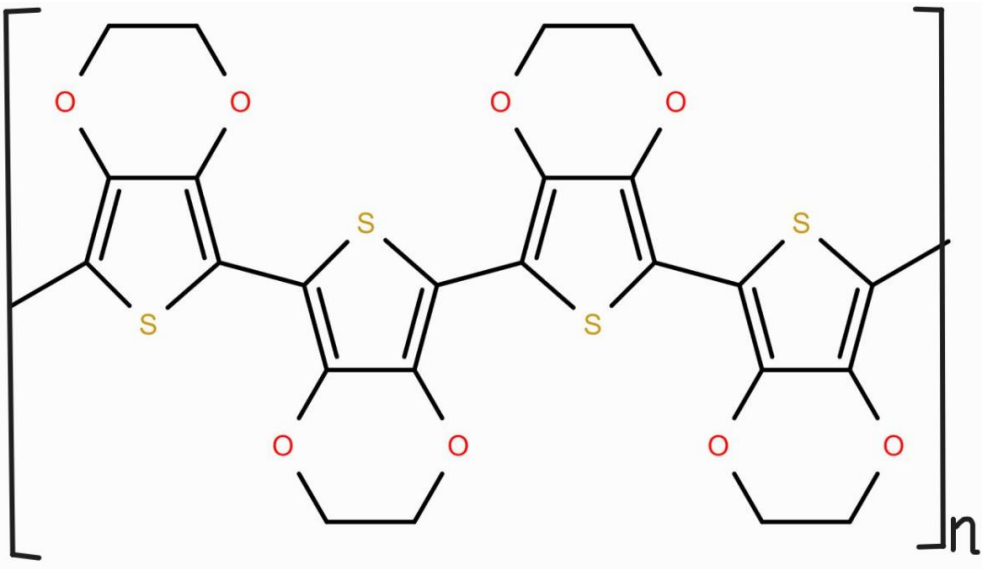

Figure 12 Molecular structures of PEDOT.

1.7 Purpose and objectives.

To improve the electrochemical performance of supercapacitors, materials science and energy storage research continue to prioritize the development of new and efficient electrode materials. This study focuses on creating a high-performance nanocomposite using RGO, CeO_2 and PEDOT. RGO, a conductive carbon material formed by the reduction of graphene oxide, is distinguished by

its great thermal stability, strong electrical conductivity, and large surface area, making it an ideal material for supporting electroactive components. The ability of CeO_2, a redox-active rare-earth metal oxides, to experience quick Ce^{4+}/Ce^{3+} redox transitions is well known and greatly enhances charge storage and pseudocapacitive behaviour. PEDOT is an extensively researched conducting polymer that provides mechanical flexibility, electrochemical stability, and good electrical conductivity. The RGO/CeO_2/PEDOT nanocomposite is created by combining these materials should have better electrochemical characteristics, which will increase charge storage and stability in supercapacitors.

The goal of this research is to synthesize the RGO/CeO_2/PEDOT nanocomposite using in-situ oxidation-reduction technique, chemical polymerization method without using other oxidant, and thoroughly characterised its chemical behaviour, to determine its potential as a suitable electrode material for high performance supercapacitors, this involves evaluating its specific capacitance, energy & power densities, and stability using conventional electrochemical techniques.

2. Experimental Section

2.1 Materials

Table 2 listed the substances employed during the experimental methods.

Name of the material	Manufacturer
Graphite flakes	Sigma-Aldrich
Potassium Permanganate ($KMnO_4$)	Sigma-Aldrich
Sulfuric acid (H_2SO_4,98% concentrated)	Merck
Hydrogen Peroxide (H_2O_2)	Sigma-Aldrich
Cerium (III) nitrate hexahydrate ($Ce(NO_3)\cdot 6H_2O$)	Sigma-Aldrich

Ammonium hydroxide (NH_4OH)	Sigma-Aldrich
3,4-Ethylenedioxythiophene (EDOT, > 98 %)	TCI
Nafion (5%)	Sigma-Aldrich
N-Methyl-2-pyrrolidone (NMP, 99.5%)	TCI
Sulfuric acid (H_2SO_4, 1 mol/L)	Merck
Conductive carbon black	Nanografi
Graphite sheet (99.88% purity)	Thermo Scientific

2.2 Experimental Instruments.

Table 3 shows the main experimental devices and their model and manufacturer for this thesis research work.

Table 3 Experimental equipment.

Instrument	Model	Manufacturer
Centrifuge	Biofuge stratos	Heraeus
Ultrasonic cleaner	USC-THD	Advantor
Hot plate stirrer	MR Hei-Tec	Heidolph
Vaccum oven		Memmert
UV-visible Spectroscopy		Bruker
Raman Microscopy		Bruker
X-ray photoelectron microscopy		
Potentiostat	A25352	Ivium

2.3 Preparation of graphene oxide from graphite (Hummer's method)

The modified Hummer's method was used to create graphene oxide from graphite flakes in the following steps: In a reaction flask, approximately 4 g of graphite flakes were mixed with 80 ml of concentrated sulphuric acid (H_2SO_4, 98%). To keep the temperature below 5ºC, the mixture was stirring for an hour in an ice bath. After 1 hour stirring, 12 g of potassium permanganate was added to the mixture gradually over a duration of 30 minutes in small amounts. To avoid excessive oxidation, the temperature was kept below 10 °C. The mixture was stirred continuously at RT for 48 hours to allow thorough oxidation and intercalation of $KMnO_4$ into the graphite layers. Following oxidation, 160 ml of distilled water was added to the mixture while constant stirring. The diluted liquid was heated to 80 °C and stirred for 3 hours to complete oxidation. After heating, the mixture was cooled to RT, then 40 ml of H_2O_2 mixed with 480ml of distilled water was added to end the reaction and reduce any leftover permanganate. This process transformed the mixture into a light brown or yellowish-brown slurry, indicating the presence of graphene oxide. The final product was centrifuged at 4000_{xg} and washed twice with distilled water, then washed with 5% HCl solution, finally the precipitate was washed with acetone to eliminate any organic impurities, it was dried in a vacuum oven at 35 °C for 12 hours. The dried GO powder was dispersed in 500 ml distilled water, prior to further use, the GO solution was subjected to ultrasonication to fully exfoliate the stacked GO layers.

2.4 Preparation of RGO/CeO_2 nanocomposites:

RGO/CeO2 composite was prepared using in-situ oxidation and reduction technique. 0.152 g of Ce(NO3)·6H2O was dispersed in 30 mL of distilled water, and then 30 ml of NH4OH was added to the dispersion during ultrasound irradiation. Next, 30 ml of GO (1 mg/ml) was mixed with the above solution followed by continuous stirring and ultrasound for 30 min. After that, the mixture suspension was heated to 90 °C, and 3 ml of Hydrazine Hydrate was added. The

product was separated by centrifugation after an hour of stirring, completely washed with ethanol and water, dried for 24 hours at 60ºC in a vacuum oven, and then allowed to cool to RT. Under the same circumstances, GO was reduced with hydrazine hydrate to create RGO for comparing. Ce(NO3)·6H2O was varied while all other parameters remained constant to make RGO/CeO2 composites with different CeO_2 contents. The final composites were designated as 1:1, 1:2, 1:3 RGO/CeO2, which corresponds to Ce(NO3)·6H2O amounts of 0.08 g, 0.2 g, and 0.23 g, respectively. The schematic diagram for the synthesis of GO and RGO/CeO2 is shown in Figure 13.[41]

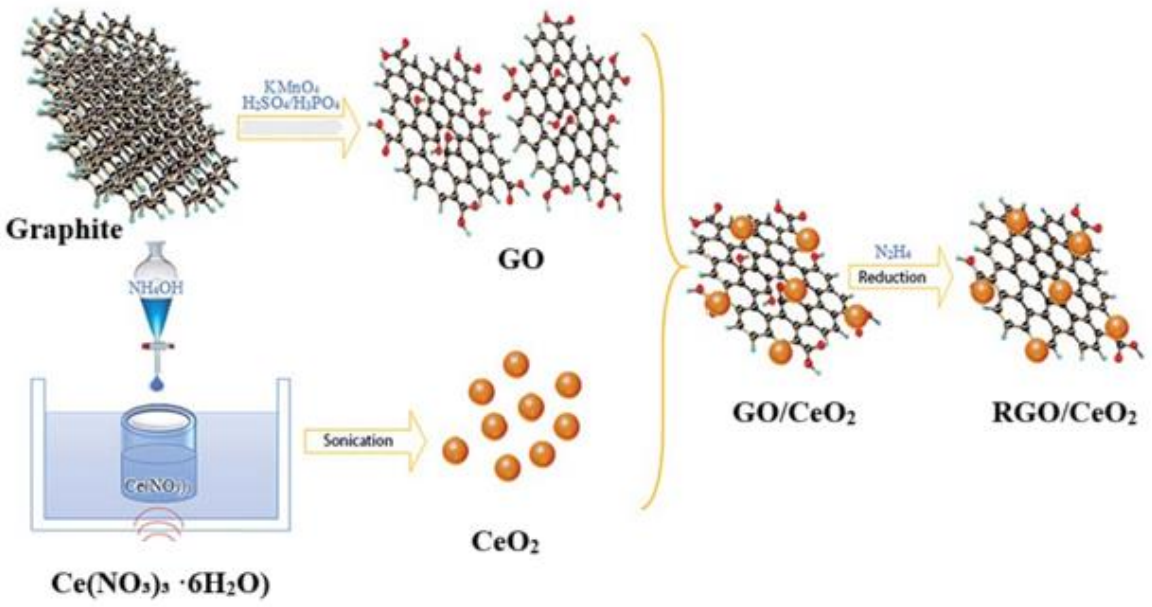

Figure 13 Schematic diagram of GO and RGO/CeO_2 composite synthesis.[41]

2.5 Preparation of RGO/CeO_2/PEDOT Nanocomposite

RGO/CeO_2/PEDOT Nanocomposite was synthesized in chemical polymerization method, 1:3 RGO/CeO_2 nanoparticles was used in this synthesize, because if it has more cerium oxide it will easily polymerize. To synthesize RGO/CeO_2/PEDOT nanocomposites, 20 mg of 1:3 RGO/CeO_2 nanoparticles were dispersed in 20 ml of distilled water, followed by sonication for 1 hour to ensure uniform dispersion. After sonication, 0.1 M H_2SO_4 was added dropwise

to the solution to adjust the pH to 2.5, with continuous sonication. Subsequently, 20 mg of 3,4-ethylenedioxythiophene (EDOT) was added to the solution and stirred for 24 hours to facilitate the polymerization. Here CeO_2 was working as oxidising agent. Centrifugation was used to isolate the final product, which was then dried for 12 hours at 60ºC in a vacuum oven before being allowed to cool to RT. Figure 14 describes the schematic diagram of RGO/CeO_2/PEDOT nanocomposites.

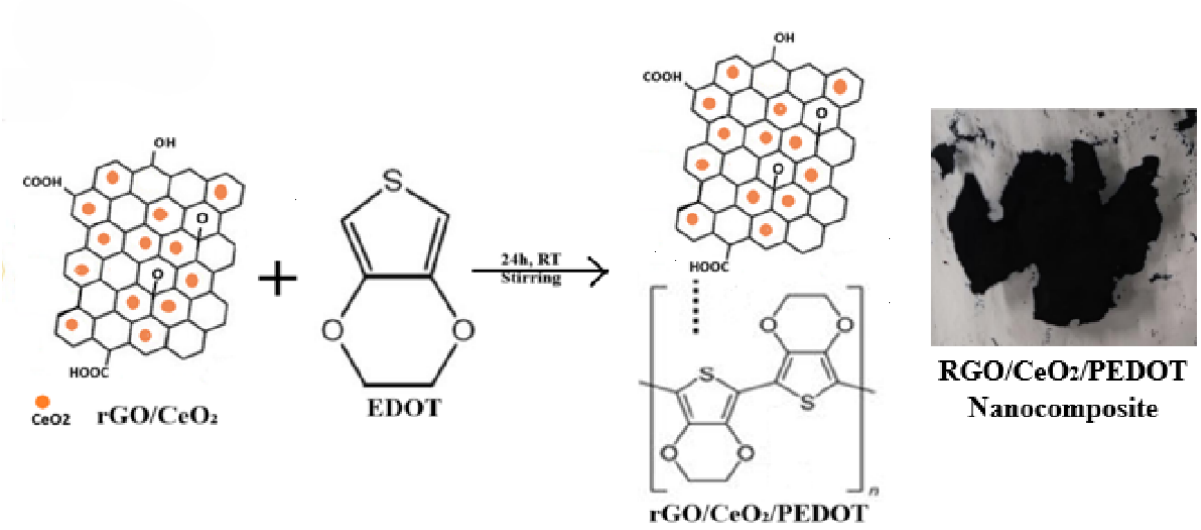

Figure 14 Schematic diagram of RGO/CeO_2/PEDOT synthesis.

2.6 Preparation of RGO/CeO_2/PEDOT electrodes

A 4 by 5 cm graphite sheet served as the substrate. 200 µl of NMP, 17 µl of Nafion, 6.4 mg of prepared composite materials, and 0.8 mg of conductive carbon were combined and mashed for 4 minutes in a mortar with pestle. Then, the mixture was then drop coated over the surface of the sliced graphite sheet and dried for 12 hours at a temperature of around 90° C. The portion coated with active material was then pressed with a pellet press at 0.5 tons for 15 seconds. After that, finished electrode was taped up so that only the coated area and the wire connecting

section were visible. It was then ready for the characterization. The Figure 15 shows the fabricated electrode.

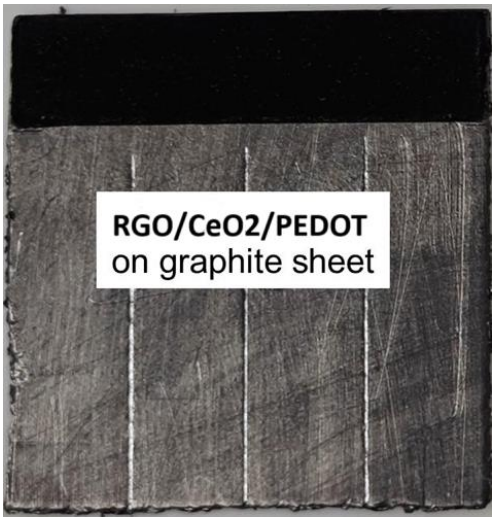

Figure 15 RGO/CeO_2/PEDOT loaded electrode.

2.7 Characterization of RGO/CeO_2/PEDOT nanocomposite.

In this study, the structural and analytical features were investigated by using Raman, UV-Vis, and XPS. Furthermore, electrochemical behaviour of prepared all the supercapacitors were examined in an electrochemical workstation.

2.7.1 UV-visible Spectroscopy

One of the fundamental analytical methods used in chemistry, the biological sciences, environmental monitoring, and industry is ultraviolet-visible (UV-Vis) spectroscopy. It is frequently used for both quantitative analysis and chemical identification based on how a substance interacts with visible (400-700 nm) and ultraviolet (200-400 nm) light. The analysis of UV-vis spectroscopy is the idea that photons of visible or ultraviolet light may be absorbed by molecules, moving electrons from lower energy molecular orbitals to higher energy antibonding orbitals. These transitions, particularly $\pi \rightarrow \pi^*$ and $n \rightarrow \pi^*$, take place in molecular systems that contain chromophores such aromatic rings, conjugated double

bonds, or certain functional groups.[42,43] The Beer-Lambert Law serves as the quantitative analysis for UV-vis spectroscopy.

$$A = \varepsilon Cl$$

$$C = A/\varepsilon l \qquad \ldots\ldots\ldots\ldots\ldots (1)$$

Where 'A' stands for absorbance(unitless). ε stands for the molar absorption coefficient ($L.mol^{-1}cm^{-1}$), C stands for the concentration of analyte (mol. L^{-1}), and l stands for the path length of the cuvette (cm).[44] For diluted solutions, absorbance is a linear function of concentration, allowing for accurate quantitative analysis. Because of this, UV-vis spectroscopy can be used to routinely determine species like organic dyes, biomolecules, and transition metals. For both qualitative and quantitative investigation, UV-vis spectroscopy is still a vital technique in the field of modern chemical, pharmaceutical, biomedical and environmental sciences.[42,44] In this experiment, the concentration of GO was determined by using UV-vis spectroscopy.

2.7.2 Raman Spectroscopy

Raman spectroscopy is an effective, non-destructive analytical method that offers in depth understanding of the vibrational, rotational, and low frequency modes of molecules using the phenomenon of inelastic (Raman) scattering of monochromatic light. The majority of photons from a laser source scatter elastically (Rayleigh scattering) when they interact with a sample, but a tiny percentage also exchange energy with molecular vibrations to produce photons with shifted energies. These energy differences correspond to distinct vibrational signatures, which effectively provide a molecular fingerprint for structural analysis and chemical identification.[45] A shift in a molecule's polarizability is required for a vibrational mode to be Raman active. Raman spectroscopy is usually used in conjunction with infrared spectroscopy because of this need, which is different from the dipole-moment change required for infrared

absorption. Two unique characteristics of the Raman effect are Stokes scattering, which produces longer wavelengths when the photon loses energy and anti-Stokes scattering, which produces shorter wavelengths when the photon acquires energy.[45,46]

The chemical environment, interactions, and molecular structure are all closely related to the locations and intensities of Raman bands. A typical spectrometer consists of a coherent laser source, and optical delivery and collection device, a spectrograph, and a sensitive detector such as CCD. Modern equipment uses notch or edge optical filters to reject Rayleigh scattering and can be set up for both point measurements and chemical imaging (Raman microscopy).[46]

In this study, the functionality of RGO, RGO/CeO_2, and RGO/CeO_2/PEDOT composite were assessed by using Raman spectroscopy, the Raman spectrometer used in the experiment is depicted in Figure 16. To guarantee a uniform particle size distribution, prepared samples were ground into a fine powder using a mortar and pestle, then the ground sample is put on a glass slide and measured with 530 nm laser running at 5% power.

Figure 16 Raman Spectrometer.

2.7.3 X-Ray Photoelectron Spectroscopy (XPS)

X-ray photoelectron spectroscopy (XPS), also known as electron spectroscopy for chemical analysis (ESCA), is a crucial surface analytical technique that allows for the quantitative and chemical state determination of elements found within the top few nanometres (1-10 nm) of a material's surface. XPS uses the photoelectric effect to irradiate a material and measure the kinetic energy of the released photoelectrons. Each element produces distinctive core-level peaks whose exact binding energies depend on the chemical environment of the atom. This makes it possible to identify elements as well as their bonding structures and oxidation states. Because of its excellent quantitative capabilities, XPS can be used to determine atomic percent compositions, compound stoichiometry, and even the thickness of ultra-thin films or overlayers by reducing underlying signals. Considering the short inelastic mean free path of photoelectrons in materials, the probing depth is naturally surface-specific, which makes XPS an essential tool for studying corrosion products, thin films, nanostructures, surface segregation, catalytic interfaces, and adsorbed biomolecules.[47,48]

In this study, the XPS equipment was used to analyse the oxidation states and surface chemical properties of RGO/CeO_2/PEDOT nanocomposites, as seen in Figure 17. To obtain uniform particle size and surface uniformity, the prepared nanocomposite was thoroughly ground with a mortar and pestle before measurement. To reduce the charging during data collection, the resultant powder was subsequently adhered to the XPS sample holder using conductive adhesive tape. The experiment was carried out with a monochromatic Al Kα radiation source under ultra-high vacuum conditions.

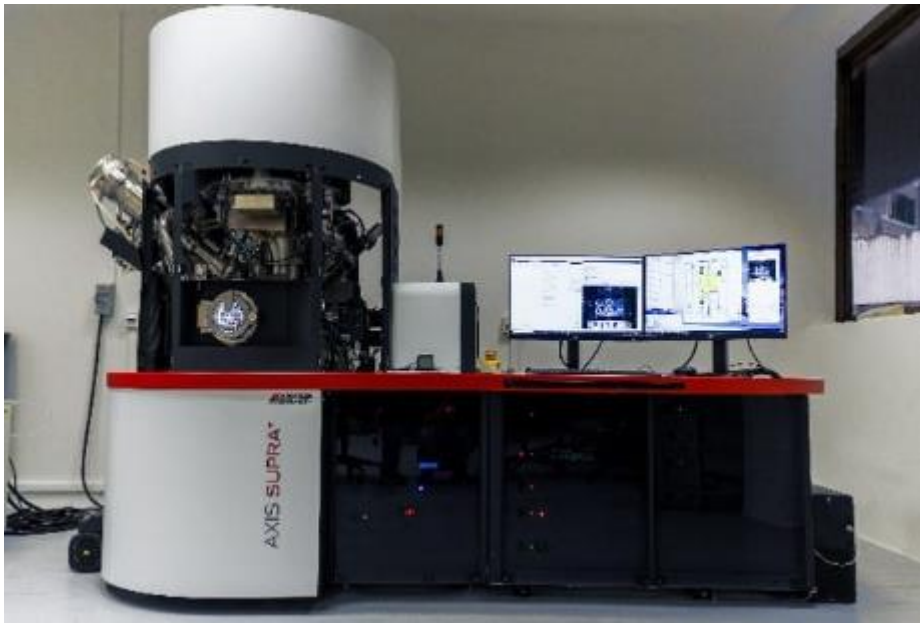

Figure 17 XPS instrument.

2.7.4 Electrochemical Workstation.

An electrochemical workstation is a sophisticated equipment used for investigating and characterizing electrochemical systems. The electrochemical workstation utilized for the measurement is seen in Figure 18. Its fundamental component is typically a potentiostat/galvanostat, which allows for the fine control of the potential (potentiostatic mode) or current (galvanostatic mode) delivered to an electrochemical cell, as well as accurate measurement of the resulting current or potential. These skills are critical for analysing processes in batteries, supercapacitors, fuel cells, electrocatalysis, biosensing, and corrosion investigations.[49] The working electrode, where the primary electrochemical process takes place, the reference electrode, which provides a stable potential reference, and the counter electrode, which completes the circuit and carries current, make up the standard electrochemical workstation interface. While monitoring current flow to or from the counter electrode, the potentiostat keeps the working electrode at a carefully regulated potential in relation to the reference. The system monitors the potential change that results from driving a steady

current between the working and counter electrodes in galvanostatic operation.[49,50]

Important analytical procedures including galvanostatic charge-discharge (GCD) and cyclic voltammetry (CV) are frequently carried out on electrochemical workstations. CV provides information on redox reactions, electron transfer kinetics, and capacitive behaviour by measuring current as a function of applied potential while sweeping potential between predetermined limits at a controlled pace. In contrast, GCD measurements, which are frequently used in supercapacitor to compute characteristics like specific capacitance and energy density, entail charging and discharging an electrode at a constant current and recording the resultant voltage-time profile. Electrochemistry is now used more widely in environmental studies, energy storage, medical diagnostics, and other fields.[51]

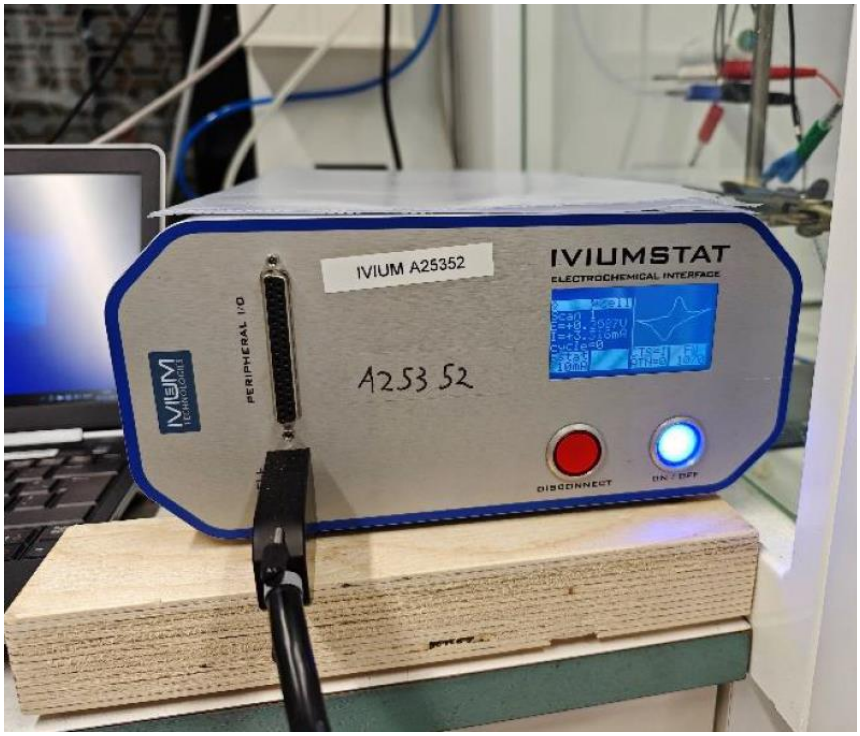

Figure 18 Electrochemical Workstation.

In this work, the electrochemical workstation, which performed the galvanic charging-discharging (GCD) and cyclic voltammetry (CV) tests, determined the

overall electrochemical performance of the RGO electrode, RGO/CeO_2 electrode, and RGO/CeO_2/PEDOT electrode under the 0.5 M H_2SO_4. The evaluated electrode active materials were put together into a three-electrode cell setup for electrochemical performance tests using a 0.5 M H_2SO_4 electrolyte. The Figure 19 illustrate the three-electrode cell setup, where working electrode is an active material, counter electrode is graphite sheet, and reference electrode is Ag/AgCl.

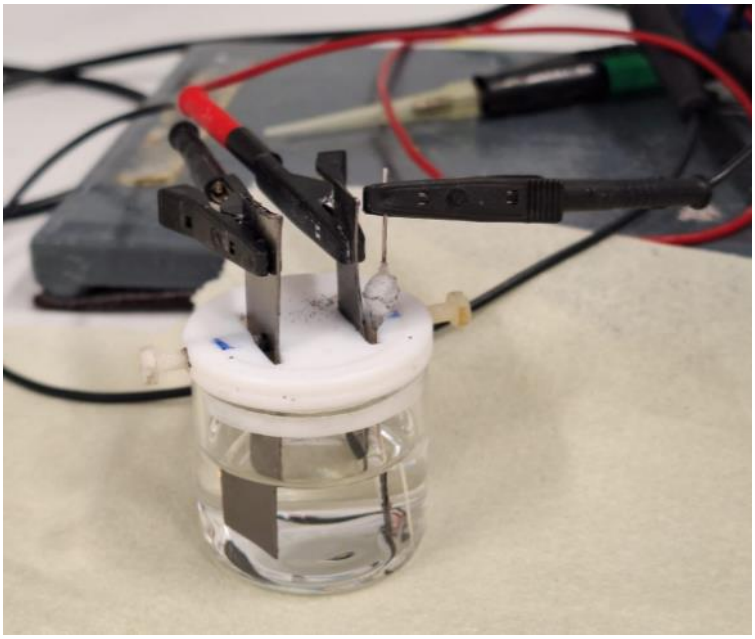

Figure 19 Three-electrode cell setup.

Within a constant potential window of -0.2 V to -0.8 V, the cyclic voltammetry measurements were conducted at a various scan speed, specifically 10 mV/s to 200 mV/s. As the same potential window, the galvanostatic charge-discharge tests were performed at different current densities ranging from 0.4 A/g to 10 A/g.

3. Results

3.1 UV-Visible Spectroscopy

The UV-visible absorption spectra of GO give important information about its electrical structure and degree of oxidation. Figure 20 shows that the GO spectrum has two distinct features, a high absorption at 230 nm, which

corresponds to the π→π* transitions of aromatic C=C bonds, a shoulder near 300 nm that is ascribed to the n→π* transitions of C=O bonds.[43] To assess the concentration of the synthesised GO solution, a dilution series was created by diluting the stock GO dispersion 100-300 times. The absorbance was measured at 300 nm, which is the typical shoulder utilized in quantitative analysis. The observed absorbance at this wavelength was 0.45. The concentration of GO stock solution was calculated to be approximately 12 mg/ml by using formula 1. This value indicates a well-dispersed and stable GO solution suitable for subsequent nanocomposite synthesis.

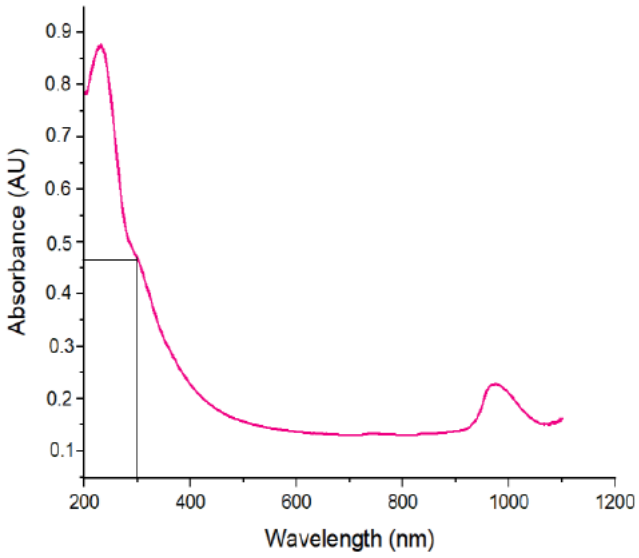

Figure 20 UV spectra of GO solution

3.2 Raman Spectroscopy

Figure 21 represents the Raman Spectroscopy data for three samples, which are RGO, 1:3 RGO/CeO_2, and RGO/CeO_2/PEDOT nanocomposite. Vibrational energy levels are represented by the Raman shift (in cm^{-1}) on the x-axis and the Raman intensity (arbitrary units) on the y-axis. The two peaks were seen for RGO, the D band at about 1342 cm^{-1} and the G band at about 1585 cm^{-1}. Graphitic domains are present because the G band is associated with the E2g vibrational

mode of sp^2 hybridised carbon atoms organised in a hexagonal lattice. Conversely, the D band corresponds to disorder and structural flaws in the graphene sheets, including edge defects, functional groups, and vacancies. In graphene materials, the intensity ratio between the D band and G band (I_D/I_G) is commonly used to evaluate the degree of reduction or graphitization as well as the concentration of defects.[52] Both the D band and G band are still present in the 1:3 RGO/CeO_2, and RGO/CeO_2/PEDOT composite, indicating that the graphene structure is maintained when CeO_2 and PEDOT incorporated.

Furthermore, a strong Raman peak was found at 461 cm^{-1} in both composite material, which is associated with the Ce-O_8 unit's symmetrical stretching vibrational mode. This distinctive peak is confirmed the presence of CeO_2 nanoparticles and their successful anchoring onto the RGO sheets.[53,54] The RGO/CeO_2/PEDOT nanocomposite's Raman spectra showed further unique characteristics. The symmetric stretching of the Cα=Cβ (-O) bond and the stretching of the Cα=Cβ bond in the PEDOT backbone are responsible for the two additional peaks that were seen at 1432 cm^{-1} and 1509 cm^{-1}, respectively.[39] The proper integration of PEDOT into the composite is unquestionably confirmed by the simultaneous existence of the D, G and PEDOT specific bands. Strong interactions between RGO, CeO_2 and PEDOT are indicated by shift, intensity modulation, and broadening of Raman peaks throughout the series.

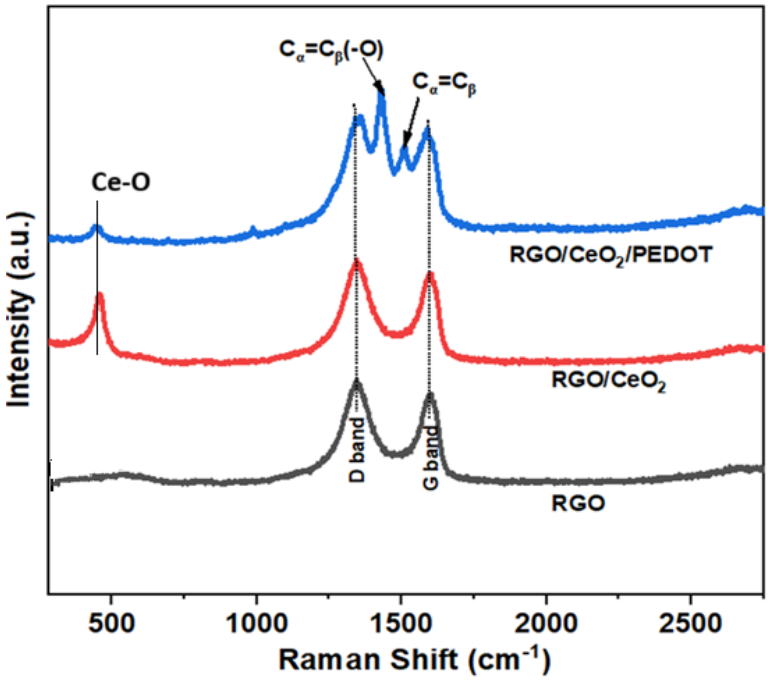

Figure 21 Raman Spectra of prepared samples.

3.3 XPS

The RGO/CeO_2/PEDOT composite was thoroughly characterized by the XPS, which validate its elemental composition, chemical states, and effective integration of the targeted components. Figure 22(a) illustrates the survey spectrum of the composite, which shows the distinct peaks for the characteristic peaks for Ce 3d, O 1s, C 1s and S 2p, corresponding to cerium, oxygen, carbon, and sulphur, respectively, which are the specific elements of CeO_2, RGO, and PEDOT.

Several peaks attributed to the Ce^{3+} and Ce^{4+} oxidation states, as well as resolved Ce $3d_{5/2}$ and Ce $3d_{3/2}$ features, are visible in the high-resolution Ce 3d spectrum as shown in Figure 22(b). Cerium oxide's oxygen vacancies and mixed valence states, which are known to improve redox behaviour and interfacial charge transfer, which aspects required for high-performance electrochemical applications are supported by the simultaneous presence of Ce^{3+} and Ce^{4+}.[56]

Lattice oxygen in CeO_2 (Ce-O), C-O-C or C=O functionalities from RGO and PEDOT, and chemisorbed or surface adsorbed oxygen are the three components that can be used to meet the O 1s area as shown in Figure 22(c). The overlapping contributions of oxygen in all three phases give rise to the broadness of O 1s, which reveals a chemically integrated interface between PEDOT, the conductive RGO scaffold and CeO_2 nanoparticles.[39,56]

Categorized peaks corresponding to sp^2 hybridised C-C/C=C bonds (~284.6 eV), C-O/C-S bonds (~285.8 eV), C=O (~287 eV), and O-C=O (~288.6 eV) can be seen in the C 1s high resolution spectra as shown in Figure 22(d). While the different oxidized carbons and C-S peaks show efficient reduction and the inclusion of PEDOT and ceria-derived oxygen functions, the dominating sp^2 signal verifies the continued existence of the conjugated graphene structure. The diversity of carbon species indicates an important chemical coupling or electrical interaction between RGO and other phases.[56,57]

The S 2p high resolution spectra as shown in Figure 22(e) contains components at ~163.5 eV (S $2p_{3/2}$) and ~164.7 eV (S $2p_{1/2}$), which are characteristic peak for sulphur atoms in the thiophene unit of PEDOT and sulphate unit of H_2SO_4. Secondary components could indicate the presence of oxidized or firmly bonded sulphur compounds due to PEDOT structural interactions with CeO_2, and RGO. The XPS results indicate the coexistence of Ce^{3+}/Ce^{4+} redox pairs, numerous oxygenated functionalities, preservation of the graphene framework, and the chemical fingerprint of PEDOT. This confirmed the effective integration of the ternary RGO/CeO_2/PEDOT composite.[39,57]

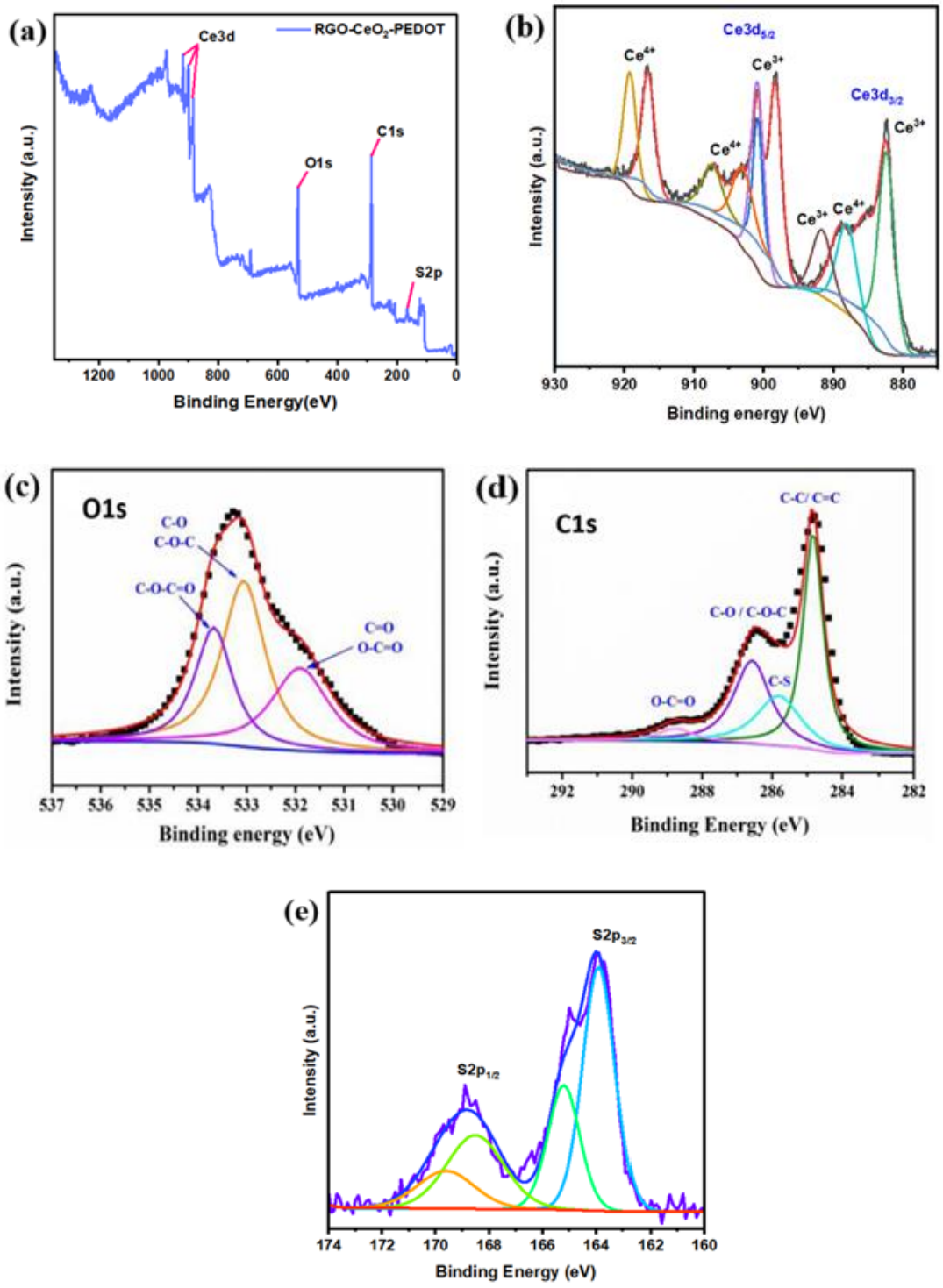

Figure 22 (a) XPS spectra of RGO/CeO_2/PEDOT composite, high resolution spectra of (b) Ce 3d, (c) O 1s (d) C 1s and (e) S 2p.

3.4 Electrochemical characterisation of RGO, RGO/CeO_2 and RGO/CeO_2/PEDOT supercapacitors.

The electrochemical performance of the prepared supercapacitors was tested using CV in a 0.5 M H_2SO_4 electrolyte within a three-electrode system. Figure 23 shows the CV curve for RGO, 1:3 RGO/CeO_2 and RGO/CeO_2/PEDOT supercapacitors at scan rates ranging from 10 mV/s to 200 mV/s. The CV curve of RGO supercapacitor (Figure 23a) displays a quasi-rectangular shape, indicating the EDLC behaviour inherent to high surface area graphene-based materials. The 1:3 RGO/CeO_2 supercapacitor (Figure 23b) has a higher current response and a bigger enclosed curve area than RGO. The presence of CeO_2 causes the pseudocapacitive behaviour through redox transitions between Ce^{4+} and Ce^{3+}. These Faradaic processes increase charge storage capacity by chemically contributing to RGO's physical double-layer capacitance. The CV plots of RGO/CeO_2/PEDOT supercapacitor illustrate the increased current density and more visible redox peaks, further indicating a significant pseudocapacitive behaviour from PEDOT. The broad, symmetrical shape of the CV curve indicates strong reversibility and rapid electron/ion transport at the electrode/electrolyte interface as shown in Figure 23c. Figure 23e illustrate the CV curves for different ratios of RGO/CeO_2 composites at a scan rate of 10 mV/s in 0.5 M H_2SO_4 electrolyte solution, 1:3 RGO/CeO_2 composite has the high current density among the three ratios, indicating better electrochemical performance. Increasing the CeO_2 content enhances the electrochemical activity of the composite. A comparison at a scan rate of 10 mV/s (Figure 23d) clearly confirms the RGO/CeO_2/PEDOT supercapacitor performs better in terms of current density and curve area than both RGO and 1:3 RGO/CeO_2. These results demonstrate that RGO/CeO_2/PEDOT is a promising electrode material for supercapacitor applications.

The GCD plots of RGO, 1:3 RGO/CeO_2 and RGO/CeO_2/PEDOT supercapacitors with 0.5 M H_2SO_4 electrolyte are displayed in Figure 24 over a range of current densities, from 0.4 A/g to 10 A/g. The conclusions derived from the CV curve can be further supported by these GCD plots.

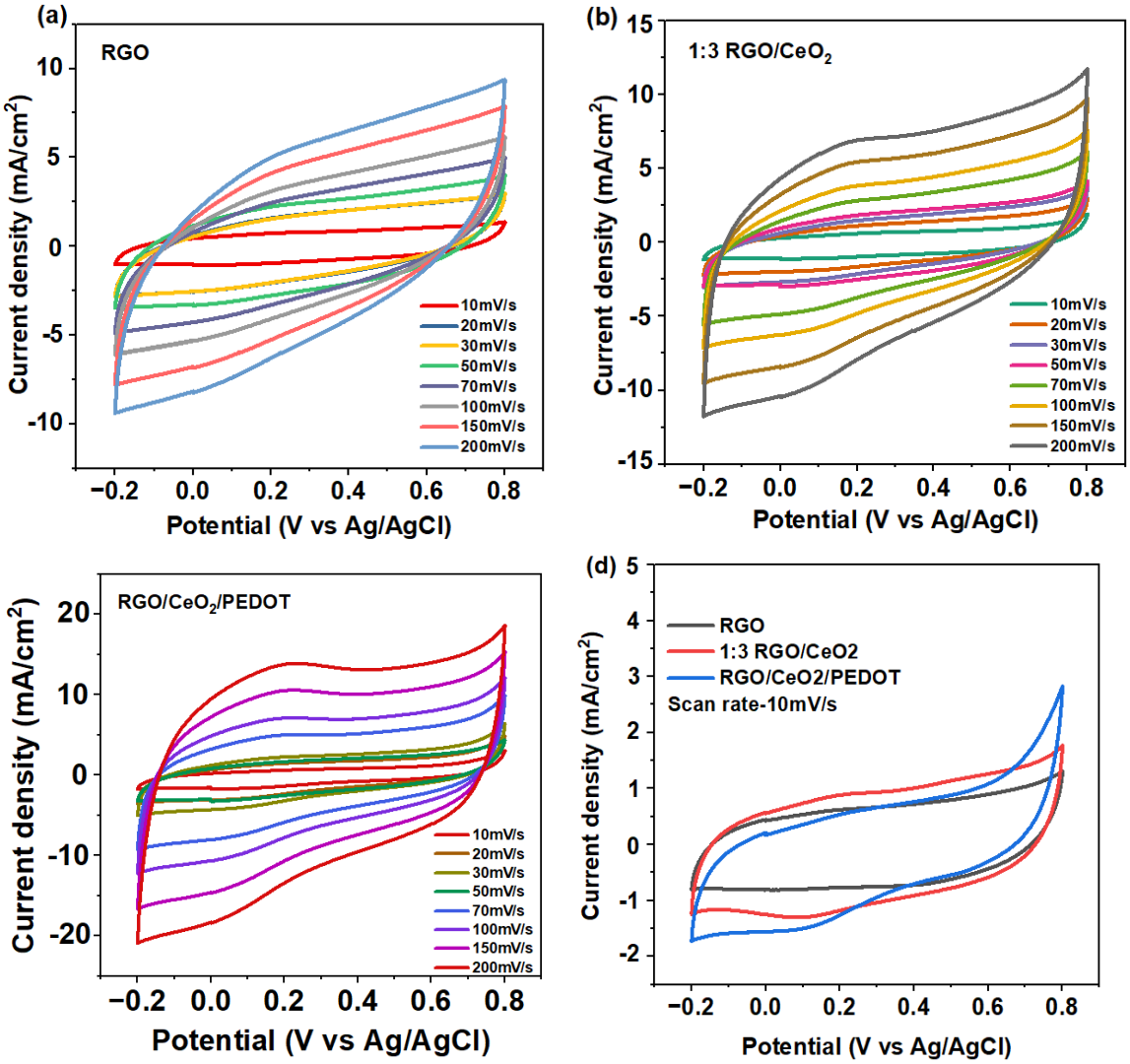

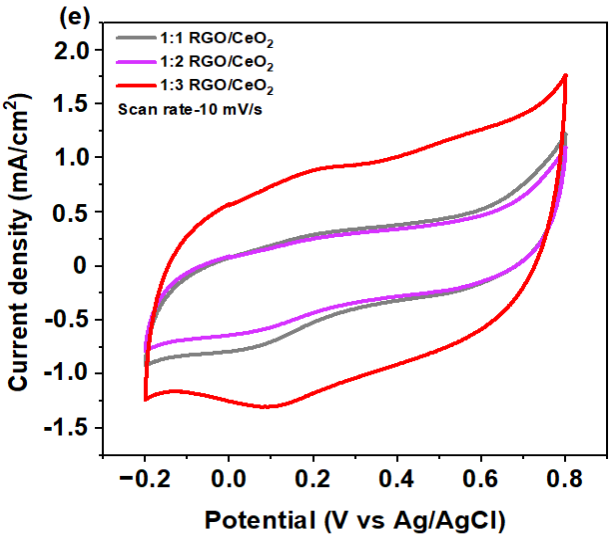

Figure 23 CV plots of (a) RGO, (b) 1:3 RGO/CeO_2, (c) RGO/CeO_2/PEDOT supercapacitors in 0.5 M H_2SO_4 electrolyte ranging from 10 mV/s to 200 mV/s and (d) Comparison of all the supercapacitors in 0.5 M H_2SO_4 at the scan rate of 10 mV/s (e) Comparison of three ratios of RGO/CeO_2 supercapacitor.

The GCD plots of RGO, RGO/CeO_2 and RGO/CeO_2/PEDOT supercapacitors with 0.5 M sulphuric acid electrolyte are displayed in Figure 24 over a range of current densities, from 0.4 A/g to 10 A/g. The conclusions derived from the CV curve can be further supported by these GCD plots.

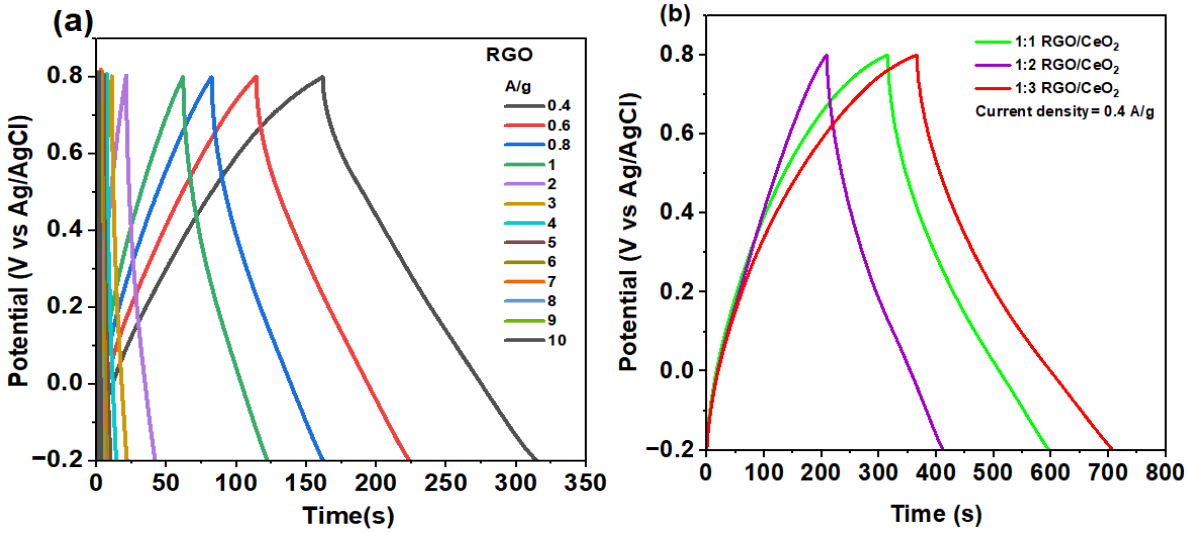

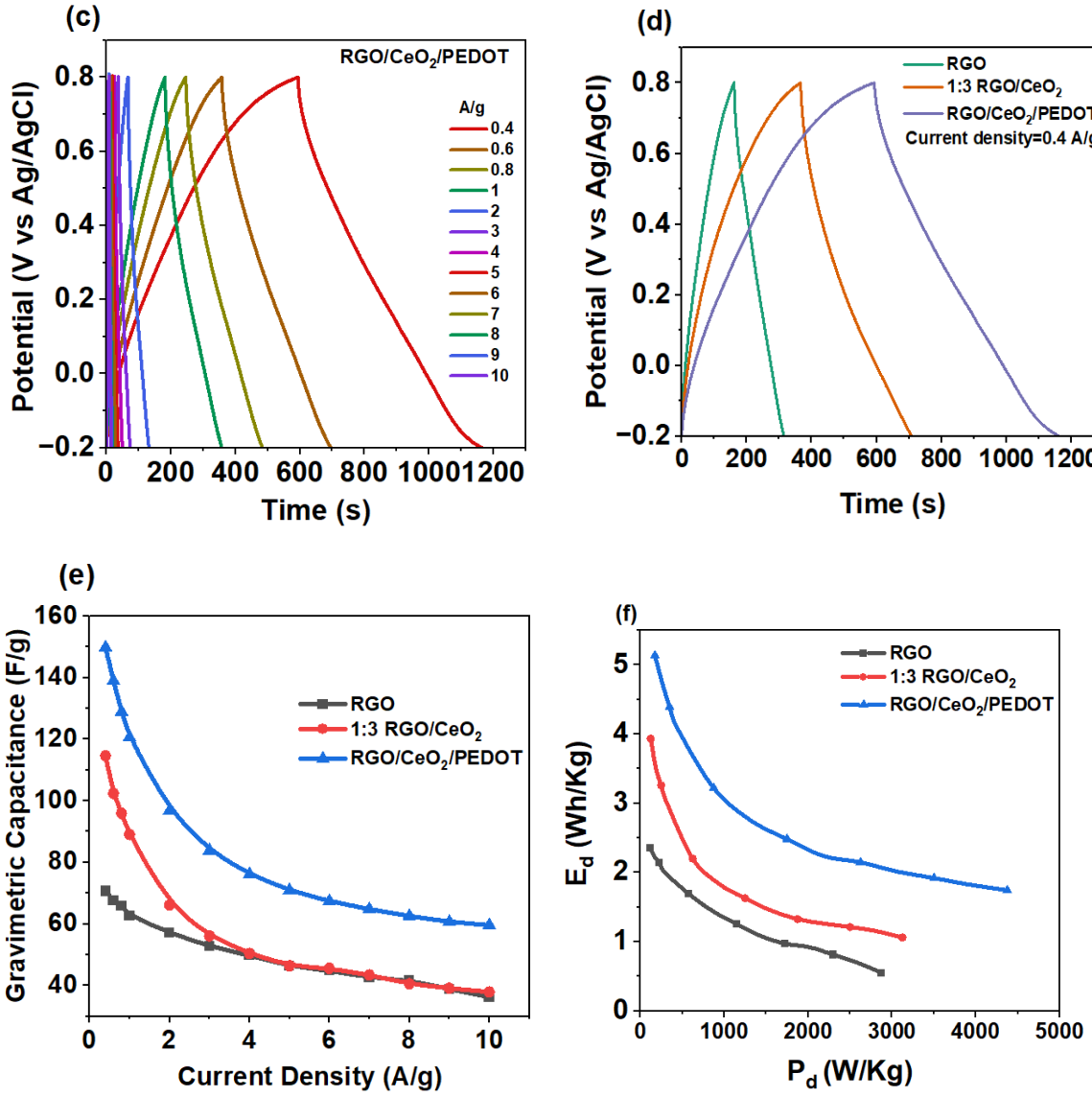

Figure 24 (a) GCD plots of RGO supercapacitor, (b) comparison of 1:1, 1:2 & 1:3 RGO/CeO_2 supercapacitors at current density of 0.4 A/g, (c) RGO/CeO_2/PEDOT supercapacitor in 0.5 M H_2SO_4 electrolyte at various current densities ranging from 0.4 A/g to 10 A/g, (d) comparison of RGO, 1;3 RGO/CeO_2 and RGO/CeO_2/PEDOT supercapacitors at a current density of 0.4 A/g. (e) Plot of current density versus gravimetric capacitance. (f) Plot of energy density versus power density.

The GCD measurements were used to calculate the specific gravimetric capacitance values of the prepared RGO, 1:1, 1:2 & 1:3 RGO/CeO_2, and RGO/CeO_2/PEDOT supercapacitors using equation 2, which were 70 F/g, 97 F/g,

83 F/g, 115 F/g and 150 F/g respectively at a current density of 0.4 A/g, Figure 24 (a to d) displays these results, every measurement was carried out using a three-electrode setup in an 0.5 M H_2SO_4 electrolyte. It is evident from Figure 24e that the RGO/CeO_2/PEDOT supercapacitors' capacitance value was higher than that of the RGO and 1:3 RGO/CeO_2 supercapacitors. These capacitance values match up with reported literature, as PEDOT/graphene and CeO_2-based composites typically have capacitances of 100-180 F/g.[26,33] Sagadevan et al. reported 145 F/g for RGO/CeO_2,[54] while Ahmed et al. achieved approximately 140 F/g using PEDOT/rGO.[39] These comparisons confirm the competitive performance of the new advanced material.

$$\text{Capacitance } C = I_{discharge}/(dV/dt)$$

$$\text{Specific gravimetric capacitance } C_G = 2 \times \frac{C}{M} \qquad \ldots\ldots\ldots\ldots\ldots (2)$$

Where C_G is the gravimetric capacitance of the active material in an electrode in F/g, M is the mass of each electrode in grams (g), $I_{discharge}$ is the discharge current in mA, and dV/dt is the slope of the discharge curve excluding the voltage (IR) drop in V/s.

$$E_{d.G} = \frac{1}{8} C_G \times V^2 \times \frac{1000}{3000}$$

$$P_{d,\,G} = E_{d.G}/t_{discharge} \times 3600 \qquad \ldots\ldots\ldots\ldots\ldots (3)$$

Where V stands for the potential window ($V\text{-}V_{IR}$) in volts (V), $E_{d,G}$ stand for the gravimetric energy density in Wh/kg, $P_{d.G}$ stands for the gravimetric power density in W/kg, $t_{discharge}$ stands for the discharge time excluding the voltage (IR) drop in seconds (s).

The energy density versus power density plots for the RGO, 1:3 RGO/CeO_2, and RGO/CeO_2/PEDOT supercapacitors are shown in Figure 24f. From there, formula 3 can be used to determine the energy and power densities of these three

supercapacitors in the presence of 0.5 M H_2SO_4 electrolyte. The RGO and 1:3 RGO/CeO_2 supercapacitors have maximum E_d and P_d values of 2.4 Wh/kg, 2785 W/kg, and 3.9 Wh/kg, 3125 W/kg, respectively. The maximum energy density and power density of the RGO/CeO_2/PEDOT supercapacitor is 5.2 Wh/kg and 4375 W/kg. It is evident from Figure 24f that the RGO/CeO_2/PEDOT supercapacitors' energy and power density increased after incorporation of PEDOT. These results demonstrated that adding CeO_2, and PEDOT to RGO improves the electrochemical performance, making it a potential material for supercapacitor applications.

4. Conclusions.

This study successfully synthesised and analysed new ternary nanocomposite made from RGO, CeO_2, and PEDOT for supercapacitor applications. RGO/CeO_2 composite was prepared by in-situ oxidation reduction technique and RGO/CeO_2/PEDOT was synthesised by chemical polymerization method and structurally characterised using UV-Visible spectroscopy, Raman spectroscopy, and XPS confirming their integration and individual contributions to the composite's functionality. The supercapacitor of RGO, 1:3 RGO/CeO_2 and RGO/CeO_2/PEDOT nanocomposite were successfully manufactured and determined within three-electrode cell setup under 0.5 M H_2SO_4 electrolyte with the help of electrochemical workstation. The specific capacitance of the RGO/CeO_2/PEDOT supercapacitor reached 150 F/g exceeding that of both RGO (70 F/g) and 1:3 RGO/CeO_2 (115 F/g) supercapacitors. The RGO/CeO_2/PEDOT supercapacitor achieved high energy and power density values of 5.2 Wh/kg and 4375 W/kg, respectively. These results support the synergistic effect of combining the high surface area of RGO, the redox activity of CeO_2, and the conductivity of PEDOT.

Overall, the RGO/CeO_2/PEDOT nanocomposite offers a viable, scalable, and eco-friendly option for enhanced supercapacitor electrode materials. Its improved electrochemical characteristics and consistent cycling behaviour make it an appealing choice for energy storage technologies designed to fulfil the growing global demand for efficient, sustainable, and fast energy delivery systems.

References

1. Jayal, N. I.; Ibrahim, R. I.; Oudah, M.K. A Review on Supercapacitors: Types and Components. J. phy. Conf. Ser. 2021, 1973, 012015.
2. Theerthagiri, J.; Senthil, R.A.; Polu, A.R.; Madhavan, J. Recent Advances in MoS2 Nanostructured Materials for Energy and Environmental Applications–A Review. J. Solid State Chem. 2017, 252, 43-71.
3. Ren, G.; Liu, J.; Wan, J.; Guo, Y.; Yu, D. Overview of Wind Power Intermittency: Impacts, Measurements, and Mitigation Solutions. Appl. Energy 2017, 204, 47-65.
4. Winter, M.; Brodd, R. J.; What are Batteries, Fuel Cells and Supercapacitors? Chem. Rev. 2004, 104, 4245-4269.
5. Wang, Y.; Song, Y.; Xia, Y. Electrochemical Capacitors: Mechanism, Materials, Systems, Characterization and Applications. Chem. Soc. Rev, 2016, 45, 5925-5050.
6. Matragostino, M.; Arbizzani, C.; Paraventi, R.; Zanelli, A.; Polymer Selection and Cell Design for Electric Vehicle Supercapacitors. J. Electrochem. Soc. 2000, 147, 407-414.
7. Chakraborty, M. N. An Overview on Supercapacitors and Its Applications. J. Electrochem. Soc. 2022, 169, 020552.
8. Allgui, A.; Fouda, M.E.; Elwakil, A.S. The Plot of Supercapacitors Under Different Loading Conditions. J Electrochem. Soc. 2020, 167, 020533.

9. Iro, Z.S.; Subramani, C.; Dash, S.S. A Brief Review on Electrode Materials for Supercapacitors. Int. J Electrochem Soc. 2016, 11, 10628-10643.
10. Zhu, Y.; Murali, S.; Stoller, M.D.; Ganesh, K.J.; Cai, W.; Ferreira, P. J. Carbon-Based Supercapacitors Produced by Activation of Graphene. Science 2011, 332, 1537-1541.
11. Sharma, P.; Kumar, V. Current Technology of Supercapacitors: A Review. J. Electron. Mater. 2020, 45, 2483-2491.
12. Kotz, R.; Carlen, M. Principles and Applications of Electrochemical Capacitors. Electrochim. Acta 2000. 45, 2483-2498.
13. Kiamahalleh, M.V.; Zein, S.H.S.; Najafpour, G.; Sata, S.A.; Buniran, S. Multiwalled Carbon Nanotubes-Based Nanocomposites for Supercapacitors: A Review. Nano, 2012. 7, 1230002.
14. Choi, H.; Yoon, H. Nanostructured Electrode Materials for Electrochemical Capacitor Applications. Nanomaterials 2015, 5, 906-936.
15. Halper, M.S.; Ellenbogen, J.C. Supercapacitors: A Brief Overview. The MITRE Corporation: McLean, VA, 2006, 1-34.
16. Simon, P.; Gogotsi, Y.; Materials for Electrochemical Capacitors. In Nanoscience and Technology: A Collection of Reviews from Nature Journals; World Scientific, 2010, 320-329.
17. Vangari, M.; Pryor, T.; Jiang, L. Supercapacitors: Review of Materials and Fabrication Methods. J. Energy Eng. 2013,139, 72-79.
18. Shinohara, H.; Tiwari, A. Graphene: An Introduction to the Fundamentals and Industrial Applications; John Wiley & Sons, Hoboken, NJ, 2015
19. Allen, M.J.; Tung, V.C.; Kaner, R.B. Honeycomb Carbon: A Review of Graphene. Chem. Rev. 2010, 110, 132-145.
20. Shareena, T.P.D. A Review on Graphene-Based Nanomaterials in Biomedical Applications and Risks in Environment and Health. Int. J. Environ. Res. Public Health 2018, 10(3), 1-34.

21. Bera, B. J. A. A Review on Polymer, Graphene and Carbon Nanotube: Properties, Synthesis and Applications. Int. J. Innov. Res. 2017, 3(10), 61-70.
22. Bhuyan, S.A.; Uddin, N.; Islam, N.; Bipasha, F. A.; Hossain, S. S. Synthesis of Graphene. Int. Nano Lett. 2016, 6, 65–83.
23. Choi, W.; Lee, J. -W. Graphene: Synthesis and Applications, CRC Press: Boca Raton, FL, 2015, 27–57.
24. Augustyn, V.; Simon, P.; Dunn, B. Pseudocapacitive Oxide Materials for High-Rate Electrochemical Energy Storage. Energy Environ. Sci. 2014,
25. Dar, M. A.; Majid, S.R.; Satgunam, M.; Siva, C. Advancements in Supercapacitor Electrodes and Perspectives for Future Energy Storage Technologies. Int. J. Hydrogen Energy 2024, 70, 10–28.
26. Bryan, A. M.; Santino, L. M.; Lu, Y.; Acharya, S.; D'Arcy, J.M. Conducting Polymers for Pseudocapacitive Energy Storage, Chem. Mater. 2016. 28, 5989-5998.
27. Del Valle, M.; Gacitúa, M.; Hernández, F.; Luengo, M.; Hernández, L. J. P. Nanostructured Conducting Polymers and their Applications in Energy Storage Devices. Ploymers 2023, 15 (6), 1450.
28. Namsheer, K.; Rout, C. S. Conducting Polymers: A Comprehensive Review on Recent Advances in Synthesis, Properties and Applications. RSC Adv. 2021, 11 (10), 5659-5697.
29. Sahin, M.E.; Blaabjerg, F.; Sangwongwanich, A. A Comprehensive Review on Supercapacitor Applications and Developments. Energies 2022, 15, 674.
30. Yetiman, S.; Pecenek, H.; Sanduvac, S. Unlocking the Potential of Bismuth-Based Materials in Supercapacitor Technology: A Comprehensive Review. ChemSusChem 2024, 17, e202400234.
31. Chamoli, P.; Banerjee, S.; Raina, K.; Kar, K. K. Characteristics of Graphene/Reduced Graphene Oxide. Handbook of Nanostructure Materials, 2023, 155-177.

32. Tarcan, R.; Todor-Boer. O.; Petrovai, I.; Leordean, C.; Astilean, S.; Botiz, I. J. Reduced Graphene Oxide Today. J. Mater. Chem. C 2020, 8 (4), 1198-1224.
33. Kowsuki, K.; Nirmala, R.; Yong-Ho, Ra.; Navamathavan, R. Recent Advances in Cerium Oxide-Based Nanocomposites in Synthesis, Characterization, and Energy Storage Applications: A Comprehensive Review. Results Chem. 2023, 5, 100877.
34. Wen, H.; Liu, Z.; Yang, Q.; Li, Y.; Yu, J. Synthesis and Electrochemical Properties of CeO2 Nanoparticle Modified TiO2 Nanotube Arrays. Electrochim. Acta 2011, 56, 2914-2918.
35. Younis, A.; Chu, D.; Li, S. Cerium Oxide Nanostructures and their Applications Funct. Nanomater. 2016, DOI:10.5772/65937.
36. Marabelli, F.; Wachter, P. Covalent Insulator CeO2: Optical Reflectivity Measurements, Phys. Rev. B, 1987, 36, 1238-1243.
37. Groenendaal, L.; Zotti, G.; Aubert, P. H.; Waybright, S. M.; Reynolds, J. R. Electrochemistry of Poly (3, 4-alkylenedioxythiophene) Derivatives. Adv. Mater. 2003, 15 (11), 855-879.
38. Anothumakkool, B.; Soni, R.; Bhange, S. N.; Kurungot, S. Novel Scalable Synthesis of Highly Conducting and Robust PEDOT Paper for a High Performance Flexible Solid Supercapacitor. Energy. Environ. Sci. 2015, 8, 1339-1347.
39. Ahmed, S.; Rafat, M. Hydrothermal Synthesis of PEDOT/rGO Composite for Supercapacitor Applications. Mater. Res. Express, 2018, 5.
40. Atanasov, S. E.; Losego, M.; Gong, B.; Sachet, E.; Maria, J.; Williams, P. S.; Parsons, G. Highly Conductive and Conformal Poly(3,4-ethylenedioxythiophene) (PEDOT) Thin Films via Oxidative Molecular Layer Deposition. Chem. Mater. 2014, 26, 3471-3478.
41. Shiralizadeh, D. A.; Ganjali, M.R.; Norouzi, P.; Faridbod, F. Facile Sonochemical Synthesis and Electrochemical Investigation of Ceria/Graphene nanocomposites. RSC Adv. 2015, 5, 30279-30285.

42. Singhal, A.; Saini, U.; Chopra, B.; Dhingra, A.; Jain, A.; Chaudhary, J. UV-Visible Spectroscopy: A Review on its Pharmaceutical and Bio-allied Sciences Applications. Curr. Pharm. Anal. 2024, 20 (in press).
43. Lai, Q.; Zhu, S.; Luo, X.; Zou, M.; Huang, S. Ultraviolet-Visible Spectroscopy of Graphene Oxides. AIP Adv. 2012, 2, 032146.
44. Malik, M.; Chan, K. H.; Azimi, G. Quantification of Nickel, Cobalt, and Manganese Concentration Using Ultraviolet-Visibles. RSC Adv. 2021, 11, 28014-28028.
45. Shipp, D. W.; Sinjab, F.; Notingher, I. Raman Spectroscopy: Techniques and Applications in the Life Sciences. Adv. Opt. Photonics, 2017, 9, 315-428.
46. Orlando, A.; Franceschini, F.; Muscas, C.; Pidkova, S.; Bartoli, M.; Rovere, M.; Tagliaferro, A. A Comprehensive Review on Raman Spectroscopy Applications. Chemosensors 2021, 9, 262.
47. Briggs, D.; Grant, J. T. Surface Analysis by Auger and XPS; IM Publications and SurfaceSpectra Ltd. Manchester, UK, 2003.
48. Watts, J. F.; Wolstenholme, J. An Introduction to Surface Analysis by XPS and AES. Surf. Interface Anal. 2003, 35, 1-10.
49. Khasim, S. Synthesis of g-C3N4/CuO Nanocomposite as a Supercapacitor with Improved Electrochemical Performance for Energy Storage applications. J. Elec. Sci. 2022, 17, 150012.
50. Feng, C.; Chen, Y.; Liu, D.; Zhang, P. Conductivity and Electrochemical Performance of LiFePO4 Slurry in the Lithium Surry Battery. IOP Conf. Ser.: Mater. Sci. Eng. 2017, 207, 012024.
51. Anshori, I.; Ramadhan, I. F.; Ariasena, E.; Siburian, R.; Affi, J.; Handayani, M. A Low-Cost and Portable Potentiostat with Multi-Channel and Multi-Analysis Electrochemical Measurements. IEEE Access, 2022, 10, 112578-112593.

52. Wu, J.; Lin, M.; Cong, X.; Liu, H.; Tan, P. Raman Spectroscopy of Graphene-Based Materials and its Applications in Related Devices. Chem. Soc. Rev. 2018, 47(5), 1822-1873.
53. Kudin, K.; Ozbas, B.; Schniepp, H.; Prud'homme, R.; Aksay, I.; Car, R. Raman Spectra of Graphite Oxide and Functionalized Graphene Sheets. Nano letters 2008, 8(1), 36-41.
54. Sagadevan, S.; Mohd Rafie, J.; Johan, M. R.; Anita, L. Fabrication of Reduced Graphene Oxide/CeO2 Nanocomposite for Enhanced Electrochemical Performance. Appl. Phys. A 2019, 125, 315.
55. Beche, E.; Charvin, P.; Perarnau, D.; Abanades, S.; Flamant, G. Ce 3d XPS Investigation of Cerium Oxides and Mixed Cerium Oxide (CexTiyOz). Surf. Interface Anal. 2008, 40, 264-267.
56. Srivastava, M.; Das, A.; Khanra, P.; Uddin, M. E.; Kim, N.; Lee, J. Characterizations of in-Situ Grown Ceria Nanoparticles on Reduced Graphene Oxide as a Catalyst for the Electrooxidation of Hydrazine. J. Mater. Chem. 2013, 1, 9792-9801.
57. Shi, Y.; Zhang, Y.; Tang, K.; Song, Y.; Cui, J.; Shu, X.; Wang, Y.; Liu, J.; Wu, Y. In-Situ Growth of PEDOT/GO Nanostructures with Enhanced Electrochromic Performance. RSC Adv. 2011, 8, 13679-13685.